



# Impact of larval behaviors on dispersal and connectivity of sea scallop larvae over the northeast U.S. shelf

Changsheng Chen<sup>a,\*</sup>, Liuzhi Zhao<sup>a</sup>, Scott Gallager<sup>b</sup>, Rubao Ji<sup>b</sup>, Pingguo He<sup>a</sup>, Cabell Davis<sup>b</sup>, Robert C. Beardsley<sup>c</sup>, Deborah Hart<sup>d</sup>, Wendy C. Gentleman<sup>e</sup>, Lu Wang<sup>a</sup>, Siqi Li<sup>a</sup>, Huichan Lin<sup>a</sup>, Kevin Stokesbury<sup>a</sup>, David Bethoney<sup>f</sup>

<sup>a</sup> School for Marine Science and Technology, University of Massachusetts-Dartmouth, MA 02744, United States

<sup>b</sup> Department of Biology, Woods Hole Oceanographic Institute, MA 02543, United States

<sup>c</sup> Department of Physical Oceanography, Woods Hole Oceanographic Institute, MA 02543, United States

<sup>d</sup> Northeast Fisheries Science Center, NOAA, Woods Hole, MA 02543, United States

<sup>e</sup> Department of Engineering Mathematics and Internetworking, Dalhousie University, Halifax, NS B3J 1Y9, Canada

<sup>f</sup> Commercial Fisheries Research Foundation, RI 02874, United States

## ABSTRACT

Sea scallops (*Placopecten magellanicus*) are a highly fecund species that supports one of the most commercially valuable fisheries in the northeast U.S. continental shelf region. Scallop landings exhibit significant interannual variability, with abundances widely varied due to a combination of anthropogenic and natural factors. By coupling a pelagic-stage Individual-Based scallop population dynamics Model (hereafter referred to as Scallop-IBM) with the Northeast Coastal Ocean Forecast System (NECOFS) and considering the persistent aggregations over Georges Bank (GB)/Great South Channel (GSC) as source beds, we have examined the dispersion and settlement of scallop larvae over 1978–2016. The results demonstrated that the significant interannual variability of larval dispersal was driven by biophysical interactions associated with scallop larval swimming behaviors in their early stages. The duration, frequency, and stimulus of larval vertical migration in the ocean mixed layer (OML) affected the residence time of larvae in the water column over GB. It thus sustained the persistent aggregations of scallops in the GB/GSC and Southern New England region. In addition to larval behavior in the OML, the larval transport to the Middle Atlantic Bight (MAB) was also closely related to the intensity and duration of northeasterly wind in autumn. There was no conspicuous connectivity of scallop larvae between GB/GSC and MAB in the past 39 years except in the autumn of 2009. In 2009, the significant larval transport to the MAB was produced by unusually strong northeasterly winds. Ignoring larval behavior in the OML could overestimate the scallop population's connectivity between GB and the MAB and thus provide an unrealistic prediction of scallop larval recruitment in the region. Both satellite-derived SST and NECOFS show that the northeast U.S. shelf experienced climate change-induced warming. The extreme warming at the shelfbreak off GB tends to intensify the cross-isobath water temperature gradient and enhance the clockwise subtidal gyre over GB. This change can increase the larval retention rate over GB/GSC, facilitating enhanced productivity on GB.

## 1. Introduction

Sea scallops (*Placopecten magellanicus*), which occur on the northeast continental shelf of North America, support the most valuable wild scallop fishery in the world (Shumway and Parsons, 2016). Georges Bank (GB) is one of two areas with the highest scallop abundances in the Northwest Atlantic (Stokesbury et al., 2004; Hart and Rago, 2006; NFSC, 2018) (Fig. 1). Based on drop-camera surveys with a coverage area of  $27 \times 10^3 \text{ km}^2$  over the period 2016–2018, Stokesbury and Bethoney (2020) estimated the scallop population over the northeast shelf, accounting for ~34 billion individual scallops, ~71% of which were on GB. Over GB, the scallop landings exhibited considerable interannual variability, with an annual value of hundreds of million dollars (Naidu and Robert, 2006; NFSC, 2018). Benefiting from the implementation of closed areas as well

as fishing effort and gear restrictions, U.S. sea scallop stocks rapidly recovered from a period of severe overfishing during the 1990s (Davis et al., 2015; Hart et al., 2013; Hart and Rago, 2006; Murawski et al., 2000; NFSC, 2018). However, even in light of the recovery, sea scallop abundances have varied significantly, largely due to high recruitment variability affected by a combination of anthropogenic and natural factors (Hart and Rago 2006; NFSC, 2018).

Recruitment, which is estimated by the survivorship of scallop larvae in their early life stages, is crucial in determining the population size. The early scallop life stages consist of pelagic and benthic phases. Adult scallops spawn eggs near the bottom. After external fertilization, trochophores hatch within 1–2 days, develop small cilia a few hours after hatching, and then start to migrate upward towards the sea surface (McGarvey et al., 1992; Hart and Chute, 2004; Cragg, 2006). Once

\* Corresponding author.

<https://doi.org/10.1016/j.pocean.2021.102604>

Received 11 January 2021; Received in revised form 21 April 2021; Accepted 6 May 2021

Available online 13 May 2021

0079-6611/© 2021 Elsevier Ltd. All rights reserved.

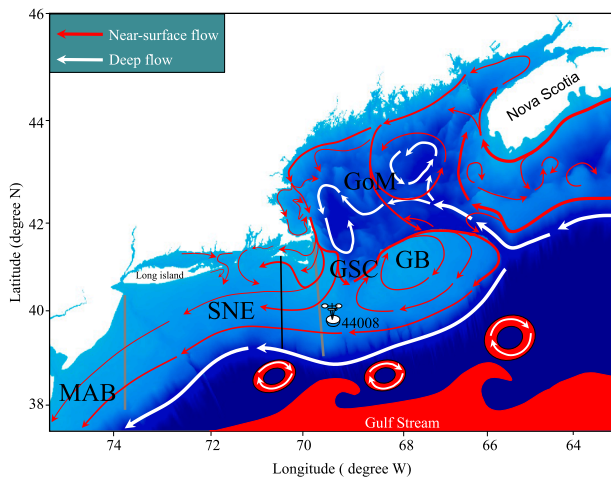


**Fig. 1.** Schematic of the near-surface (red arrows) and deep (white arrows) flows over the US northeast shelf. GB: Georges Bank, GSC: Great South Channel, SNE: Southern New England, MAB: Middle Atlantic Bight. The red color patch represents the Gulf Stream northward meander water. Red color rings represent the warm-core ring separated from the Gulf Stream. Gray thick lines are the boundaries between GB/GSC, SNE, and MAB. The solid black thin line is the transect where the transport was calculated. The 3-D icon represents the NOAA buoy, and the number on the right is the buoy number. (For interpretation of the references to color in this figure legend, the reader is referred to the web version of this article.)

arriving at the sea surface, they undergo vertical migrations within the surface oceanic mixed layer (OML) (Tremblay and Sinclair, 1990a, 1990b; Gallagher et al., 1996). The veliger stage is reached over 4–5 days with the development of shell velum (Silva-Serra, 1995; Pearce et al., 2004). At the ages of 30–35 days, veligers develop into pediveligers with foot and byssus development (Stewart and Arnold, 1994). Pediveligers can actively swim across the thermocline and descend towards the bottom for settlement (Tremblay et al., 1994). During this pelagic phase, changes in the flow-driven larval dispersal and retention are primary factors in controlling interannual variability in spatfall and abundance (McGarvey et al., 1993). After settlement, the survivorship of spat (settled larvae) and juveniles crucially influences the adult sea scallop population size and distribution (Caddy, 1975; Hart and Chute, 2004). During this benthic phase, the substrate motility, water temperature, currents/storms, predation, and starvation can affect the survivorship of newly settled spat and juveniles (Merrill and Edwards 1976; Larsen and Lee 1978, Hart 2006, Shank et al., 2012).

The interannual variability of scallop abundance and recruitment on GB/GSC is influenced considerably by changes in both physical and biological processes (Hart and Chute, 2004). Understanding the driving mechanisms of these variabilities and their connectivity with the Middle Atlantic Bight (MAB) can provide insights into the biophysical reasons for persistently high scallop abundance over GB/GSC and primary factors attributing to abundance reductions. It can also scientifically guide the management of rotationally closed areas, optimal seeding of sea scallops, and protection of seeded sea scallop's settling regions. It is a significant challenge to predict environment-driven variability in the GB/GSC scallop population. The environmental factors reflect the complex nonlinear physical-biological interaction processes, such as global warming, climate-induced shelf-basin scale interactions, local wind/tidal mixing, ocean acidification, ecosystem regime shift, and prey/predator fields, etc. (Hart and Rago, 2006; Shank et al., 2012; Stokesbury et al., 2016; Rheuban et al., 2018).

The sea scallop fishery in the U.S. Northeast is currently managed using fishing effort limitations combined with rotational closures (Hart and Rago 2006). Areas are closed based on observations of strong recruitment from surveys, and then reopened to fishing after the scallops

have grown to more optimal sizes for harvesting. There have been a few modeling studies carried out to assess the marine environmental impact on recruitment processes (reproduction, the timing of spawning, pre and post-settling larval stages) on GB/GSC (Davis et al., 2015; Gilbert et al., 2010; Tian et al., 2009a–c) and in the MAB (Munroe et al., 2018, Hart et al., 2020). Tian et al. (2009a) developed a scallop population individual-based model (hereafter referred to as Scallop-IBM). The model was coupled with the unstructured grid, Finite-Volume, Community Ocean Model (FVCOM) for the Gulf of Maine (GoM) (hereafter referred to as GoM-FVCOM) (Tian et al., 2009a, 2009b, 2009c). Spawning on GB in autumn, they ran this coupled Scallop-IBM/GoM-FVCOM model for 1995–2005. The dispersal of simulated scallop larvae varied interannually, with significant transport to the MAB (Tian et al., 2009c). Driving a simplified passive and pycnocline-seeking, temperature-dependent, scallop larval transport model by FVCOM-simulated monthly climatological flow and temperature fields, Gilbert et al. (2010) examined the influences of flow-driven retention and larval vertical migration on the larval dispersion in the GB/GSC region for both fall and spring spawning seasons. They found that pycnocline-seeking behavior could alter the larval dispersal by factors of 2–5, and thermal history could significantly affect the planktonic larval duration.

The flow and temperature fields used in previous scallop larval transport simulations (e.g., Tian et al., 2009a, 2009b, 2009c; Gilbert et al., 2010) were from the first-generation GoM-FVCOM for the region, which did not consider the physical processes relating to regional-scale climate forcing. Specifically, the GoM-FVCOM hydrodynamics missed two remote boundary conditions: (1) the advective transport from the upstream Labrador Sea and the Arctic Ocean, and (2) the Gulf Stream-shelf interactions along the southeastern part of the domain (Fig. 1). Regarding the population dynamics, although Scallop-IBM included the pre-settling pycnocline-seeking behaviors of scallop larvae, age-at-size-specific pre- and post-settling swimming within the OML or near the bottom were not taken into account (Stewart and Arnold, 1994; Gallagher, 1996; Gallagher and Mann, 1986, Gallagher et al., 1986, 1996). Additionally, the spawning distribution for the 1995–2005 simulations was based only on a scallop dataset produced by video surveys from the University of Massachusetts/School for Marine Science and Technology (UMASS-D/ SMAST) (Stokesbury et al., 2004). This dataset does not contain the data from either the Canadian waters over the eastern flank of GB or NOAA surveys conducted independently every year with records back to 1979. The larval behaviors and spatial distributions of spawning are known to have a significant role in the bulk transport of larvae (Gilbert et al., 2010). It is necessary to conduct an in-depth analysis of the responses of dispersal patterns to different behaviors by using a model initiated with complete coverage of spawning locations from all available scallop data.

High levels of adult biomass on GB/GSC, including the closed areas over Nantucket Lightship Closed Area (NLCA), Closed Area I (CA-I), Closed Area II (CA-II), and Habitat Area of Particular Concern (HAPC) in the northern part of CA-II, are well established (Hart and Rago 2006; Hart et al., 2013; Stokesbury et al., 2015; Gallagher, 2016). For data mining, we collected the scallop abundance data from NOAA, Canadian, and SMAST surveys, and expanded the database to cover a period from 1979 to 2017. For model development, we, a joint research team at UMASS-D and Woods Hole Oceanographic Institution (WHOI), developed the Northeast Coastal Ocean Forecast System (NECOFS). The 39-year (1978–2016) hindcast simulation of NECOFS was conducted using a global-regional nested FVCOM system, which improved the numerical simulation of the regional circulation by including the Gulf Stream-shelf interaction and flows from the upstream Labrador Sea and the Arctic Ocean. The availability of a complete scallop abundance dataset and 39-year NECOFS hydrodynamic fields allows us to re-examine the influences of physical processes and scallop larval behaviors on the early life stages of scallop larvae in the region. In particular, how do the Gulf Stream-shelf interaction and flows from the upstream Labrador Sea and the Arctic Ocean influence the transport of larval in GB

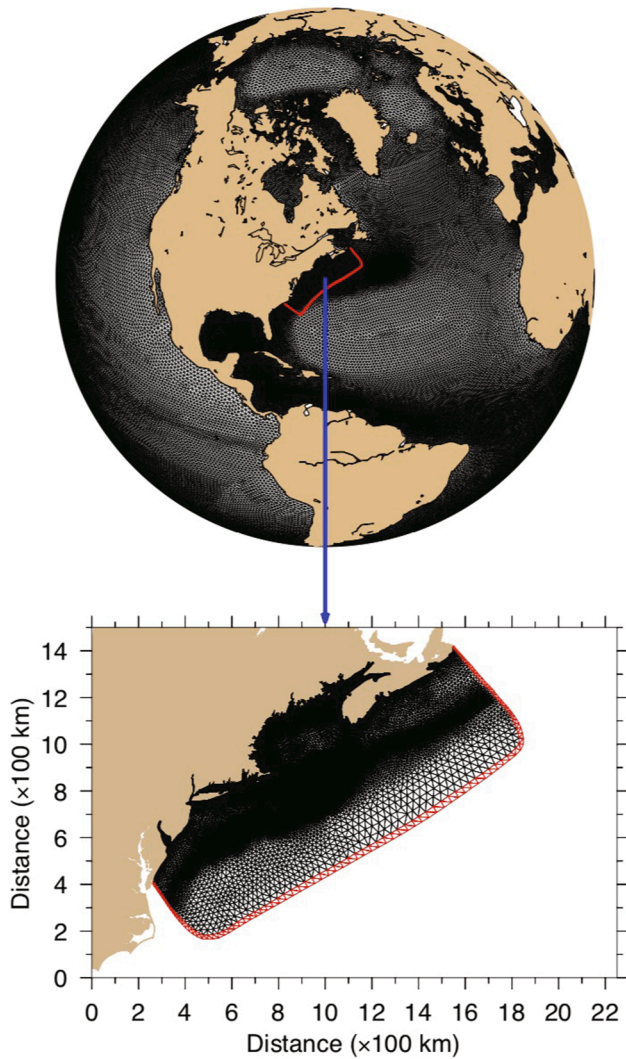


Fig. 2. The unstructured meshes for Global-FVCOM and GoM-FVCOM. The cells marked with red colors represent the common cells nesting between Global-FVCOM and GoM-FVCOM. (For interpretation of the references to color in this figure legend, the reader is referred to the web version of this article.)

and the MAB in the context of realistic larval motility? How do these factors change the population connectivity between GB, Southern New England (SNE) shelf, and the MAB compared to previous estimates? Does the short-term vertical migration affect the dispersal and settlement of scallop larvae in their early life stages? What is the relative importance of these physical and biological factors for understanding and predicting changes due to dispersal and retention? Ultimately, could a coupled physical and individual-based fishery model reproduce and predict biophysical processes in terms of interannual variability and future management implications?

In this research, we have upgraded the Scallop-IBM with improvements of larval behavior parameterizations in the pre-settling stage and coupled it with the third version of GoM-FVCOM of NECOFS (hereafter referred to as GoM3-FVCOM). Using this upgraded coupled model, we examined the dispersal and settlement of scallop larvae with eggs spawning on GB/GSC over 39 years from 1978 to 2016. The NECOFS-produced hourly physical fields include the Gulf Stream-shelf interaction and the upstream flows from the Labrador Sea and the Arctic Ocean. The simulation aimed to assess the impacts of various migrating larval behaviors within the surface OML on the scallop larvae's dispersal and settlement in their early life stages.

The remaining sections are organized as follows. Section 2 describes

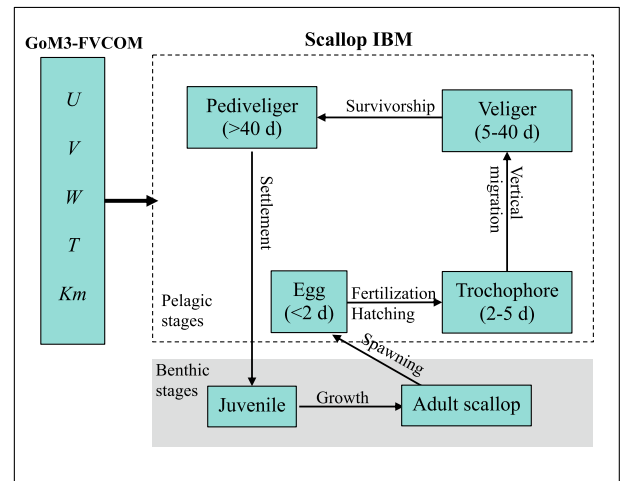


Fig. 3. Structures of the scallop-IBM early life stage model. Four pelagic stages are considered: (1) egg, (2) trochophore, (3) veliger, and (4) pediveliger.  $U$ ,  $V$ , and  $W$  are the  $x$ ,  $y$ , and  $z$  components of the water velocity.  $T$  is the water temperature, and  $K_m$  is the vertical eddy viscosity. The dashed line box presents the pelagic stages, and the gray shadow area indicates benthic stages.

the data and the model. Section 3 presents the results of model simulations, including the discussion on the sensitivity of larval dispersal and retention to larval behaviors in constant and varying OMLs and the scallop population's connectivity between GB/GSC, SNE, and MAB. Section 4 highlights the biological and physical processes affecting the interannual variability of larval dispersal. Finally, section 5 summarizes the findings with conclusions.

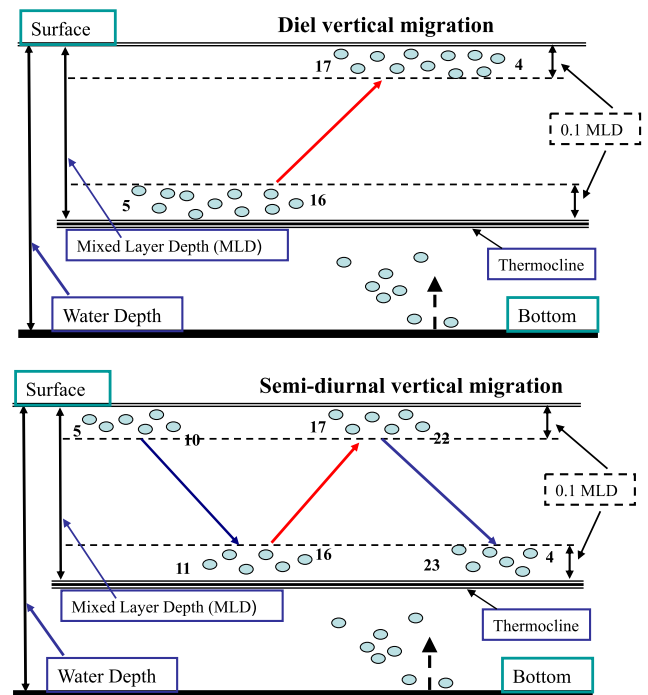


Fig. 4. The diel and semidiurnal larval vertical migration sub-models in the surface mixed layer during the period of 5 through 40 days from eggs to veliger stages. Diel and semi-diurnal vertical migration patterns were based on the observations made by Tremblay and Sinclair (1990b), Manuel et al. (1996), and Gallager et al. (1996). The number in the figure indicates the time of a day defined by a 24-hour clock.



## 2. The coupled NECOFS-scallop-IBM model and data

### 2.1. NECOFS

NECOFS is an integrated atmosphere, surface wave, and ocean forecast model system designed for the U.S. northeast coastal region. For the NECOFS version used in this study, the computational domain covers the continental shelf with boundaries over the northern coast of Chesapeake Bay on the south and the Scotian Shelf on the north, including a portion of the MAB (Fig. 2). NECOFS was placed in experimental 24/7 forecast operations in late 2007. The present version of NECOFS includes (1) a community mesoscale meteorological model named “Weather Research and Forecasting (WRF-AWR)”; (2) the regional ocean model of FVCOM (GoM3-FVCOM) (Chen et al., 2003); (3) the unstructured-grid surface wave model (FVCOM-SWAVE) with the same domain as GoM-FVCOM (Qi et al., 2009); (4) the Mass Coastal FVCOM with the inclusion of estuaries, inlets, harbors, and intertidal wetlands; and (5) four subdomain coupled wave-current FVCOM inundation forecast systems in Scituate, MA; Boston Harbor, MA; Hampton-Seabrook Estuary, NH, and Saco Bay, ME. The GoM3-FVCOM grid covers the scallop aggregation areas over GB/GSC, SNE, and the MAB. The grid is constructed using unstructured triangular meshes with a resolution of  $\sim 0.3$ – $25$  km in the horizontal and 45 layers in the vertical.

The 39-year (1978–2016) hindcast simulations of NECOFS were conducted using a global-regional nested FVCOM system with the core models of Global-FVCOM and GoM3-FVCOM (Fig. 2). Global-FVCOM is a fully coupled atmosphere-ice-wave-ocean, unstructured-grid primitive equation global ocean model with a horizontal resolution varying from  $\sim 2$  km within the Canadian Archipelago, shelfbreak, and coastal region to  $\sim 50$  km in the interior open ocean. This model was driven by (a) astronomical tidal forcing with eight constituents ( $M_2$ ,  $S_2$ ,  $N_2$ ,  $K_2$ ,  $K_1$ ,  $P_1$ ,  $O_1$ , and  $Q_1$ ), (b) surface wind stress, (c) net heat flux at the surface plus

shortwave irradiance in the water column, (d) surface air pressure gradients, (e) precipitation (P) minus evaporation (E), and (f) river discharges (Chen et al., 2016; Zhang et al., 2016a, 2016b). A 39-year NECOFS hourly hindcast product is now available on the NECOFS Web Map Server (<http://porpoise1.smast.umassd.edu:8080/fvcomwm/s/>). This database includes meteorological and oceanic components. The meteorological database includes hourly fields of physical variables such as wind velocity, air pressure, precipitation minus evaporation, shortwave radiation, longwave radiation, sensible and latent heat fluxes, and air temperature, etc. The oceanic database contains hourly fields of three-dimensional water currents, temperatures, salinity, horizontal/vertical turbulent diffusion rates, and surface elevation.

The NECOFS-simulated physical fields were validated through comparisons with available observations. It has demonstrated success in capturing tidal- and shelfbreak density fronts, residual clockwise gyres, wind-driven upwelling, buoyancy-driven river plume, the Gulf Stream-shelf interaction (e.g., warm-core rings), and volume and mass transports entering the Gulf of Maine over the Nova Scotia shelf from the upstream Labrador Sea or even the Arctic Ocean. The model-data comparisons included (1) water elevations at tidal gauges (Chen et al., 2011, Sun et al., 2013), (2) temperature and salinity in the water column (Li et al., 2015), (3) hurricane and extratropical storms (Beardsley et al., 2013; Chen et al., 2013a), (4) the surface currents measured by CODAR from 2000 to 2008 (Sun et al., 2016), and (5) upstream conditions in the Arctic Ocean (Chen et al., 2009; Chen et al., 2016; Zhang et al., 2016a, 2016b). The success of scallop-IBM depends on the accuracy and reality of the flow fields predicted by the physical model. We have conducted a model-drifter comparison to validate the reliability of the FVCOM-produced flow field over 1995–2013. Six hundred eighty-four drifters were deployed in the GoM and GB regions, which returned valuable trajectory data (J. Manning, personnel communication). A non-parametric Kolmogorov-Smirnov test was used to judge “good” and “bad” comparisons (Van Sebille et al., 2009). The results showed that 75% of drifters were in fair comparison with the model-predicted drifter trajectories (Sun, 2014). These validation experiments provide us with confidence in using the NECOFS-produced flow field to study the impact of physical processes on the interannual variability of sea scallop recruitment over GB/GSC, SNE, and MAB.

### 2.2. Scallop-IBM

The model used in this study is an upgraded Scallop-IBM coupled with the GoM3-FVCOM model. Scallop-IBM consists of four phases: egg,

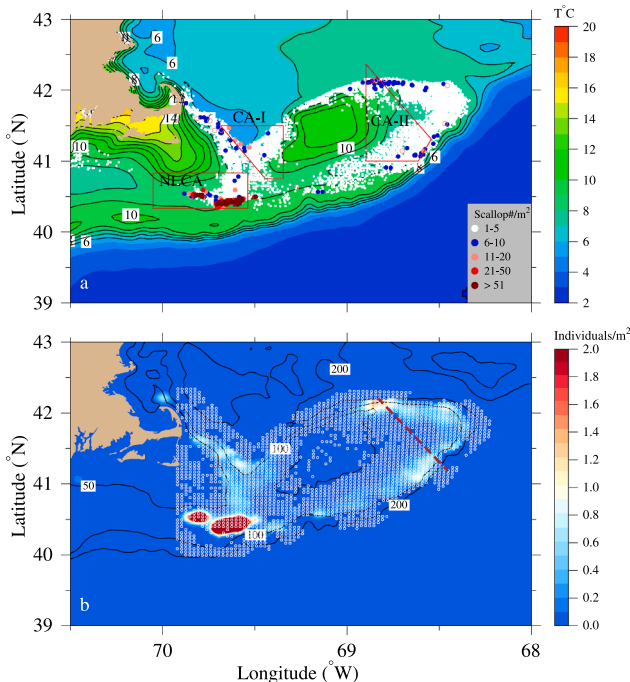


**Fig. 5.** Scallop abundance (scallop#/m<sup>2</sup>) (a) and gridded density (individual/m<sup>2</sup>) (b) for spawning. The individuals in each cell were determined using the combined scallop data from BIO, NOAA, and SMAST. In the upper panel, shapes bounded by red lines are the closed areas; CA-I: closed area I, CA-II: closed area II, and NLCA: Nantucket Lightship closed area. In the lower panel, the dashed thick line is the boundary between the US and Canadian waters. (For interpretation of the references to color in this figure legend, the reader is referred to the web version of this article.)

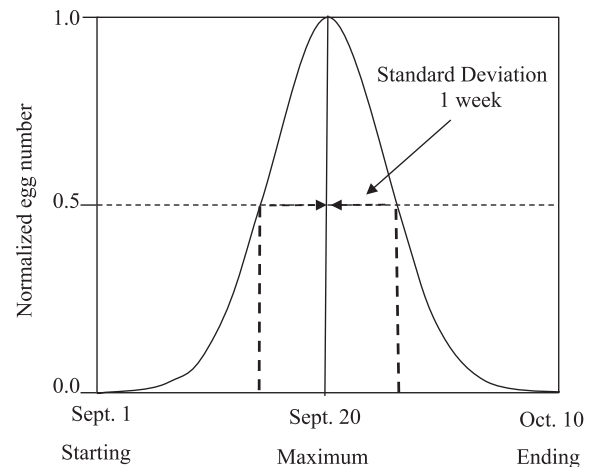


**Fig. 6.** Illustration of the egg spawning period starting at 00:00 September 1 and ending at 24:00 October 10. The spawning process satisfies a normal probability distribution with the maximum on September 20 and a one-week standard deviation.



**Table 1**

Types of numerical experiments made in this study.

Parameters		
Case	OML	Larva behavior
Case 1 (C#1)	No	No
Case 2 (C#2)	10 m	diel migration
Case 3 (C#3)	10 m	semidiurnal migration
Case 4 (C#4)	30 m	diel migration
Case 5 (C#5)	30 m	semidiurnal migration
Case 6 (C#6)	varying	diel migration
Case 7 (C#7)	varying	semidiurnal migration
Case 8 (C#8)	varying	thermocline-seeking

trochophore, veliger, and pediveliger (Fig. 3). Ages defined individual development in each stage: eggs < 2 days, trochophores 2–4 days, veligers 5–40 days, and pediveligers > 40 days (Stewart and Arnold, 1994). We used fixed development times on pelagic stages under the assumption that the relatively small interannual changes in water temperature would produce insignificant modulation in larval development times. Similarly, the food limitation was not considered for larvae since that food was abundant during the pelagic stages.

Modeled larval behavior and their vertical migrations were considered for each life stage based on our empirical understanding. Eggs are spawned on the seabed, neutrally buoyant, and drift passively via vertical currents and turbulence but without vertical migration (Culliney,

1974; Silva and O'Dor, 1988; Tremblay, 1988; Tremblay et al., 1994). Trochophores have no directionality in their swimming and only randomly spin (Tian et al., 2009a), and so were also treated passively. Laboratory experiments have found that once the first shell formed (*prodisoconch*) and the larvae appear in a 'D' configuration, their gravity centers are below the velum, causing them to swim upwards across the thermocline (Gallager, 1993; Gallager et al., 1996). Veligers are subject to horizontal drift in the surface OML above the thermocline, in which they actively switched between upward swimming and sinking to produce a distinct vertical migration pattern. Veligers are sensitive to light transitions, not to any prolonged state of light intensity like day or night (Gallager et al., 1996). Larvae between the ages of 5 and 40 days vertically migrate within the OML with various patterns such as thermocline-seeking aggregation (Tremblay and Sinclair, 1990a), diel (Tremblay and Sinclair, 1990b), and semidiurnal cells (Gallager et al., 1996; Manuel et al., 1996). Tremblay and Sinclair (1990b) used a pump to make profile samplings of scallop larval abundance at eight stations on GB in October 1986 and 1987, respectively. Four of the stations were located in the stratified region. They observed an aggregation of bivalve scallop larvae in the thermocline at a depth of the subsurface chlorophyll maximum. In laboratory mesocosm experiments, over a diel cycle, veligers stayed near the surface at night, moved down, and remained at the thermocline during the day (Manuel et al., 1996) (Fig. 4). Over semidiurnal migration cycles, they stayed near the surface when daybreak, moved to the thermocline around noon, came up towards the surface at

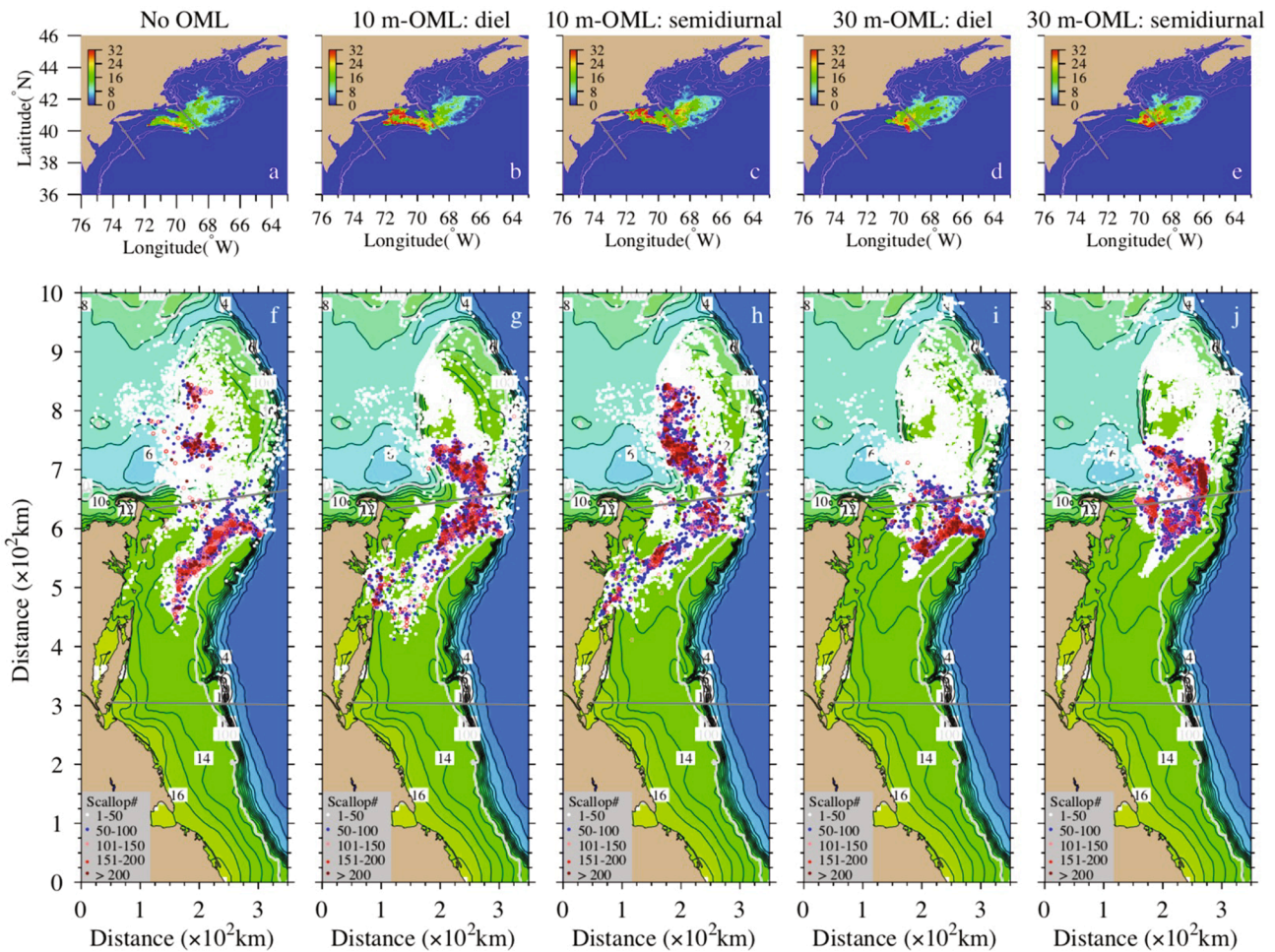


**Fig. 7.** Distributions of the settled larval density (a-e) and locations/ abundances of settled super-individuals (f-j) for the cases C#1 (No OML), C#2 (10 m-OML: diel), C#3 (10 m-OML: semidiurnal), C#4 (30 m-OML: diel), and C#5 (30 m-OML: semidiurnal). The results were from the 2008 simulation. Two thick gray lines are the boundaries between GB/GSC, SNE, and MAB. Gray lines with labels are 50, 100, and 200-m isobath contours.

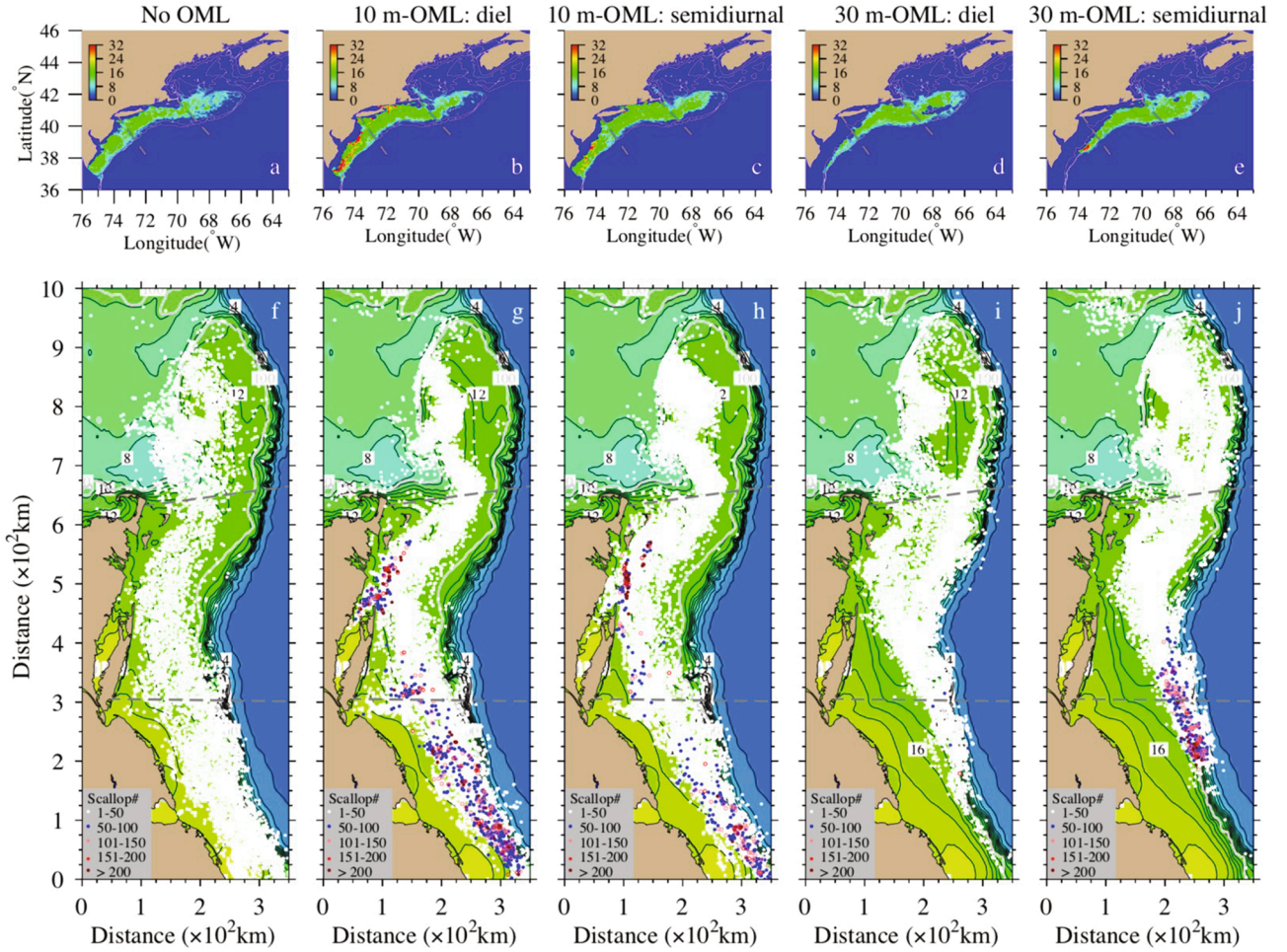


**Fig. 8.** Distributions of the settled larval density (a-e) and locations/ abundances of settled super-individuals (f-j) for the cases C#1 (No OML), C#2 (10 m-OML: diel), C#3 (10 m-OML: semidiurnal), C#4 (30 m-OML: diel), and C#5 (30 m-OML: semidiurnal). The results were from the 2009 simulation. Two thick gray lines are the boundaries between GB/GSC, SNE, and MAB. Gray lines with labels are 50, 100, and 200-m isobath contours.

sunset, and were back to the thermocline around mid-night, forming bio-convective cells within the OML after dark (Manuel et al., 1996) (Fig. 4). Larvae also respond to turbulence's ephemeral pulses  $>10^{-7} \text{ W} \cdot \text{Kg}^{-1}$  by withdrawing their velum and sinking rapidly until the turbulent energy has subsided (Pearce et al., 1998). The currents in the GB/GSC region are dominated by the semidiurnal  $M_2$  tidal currents. During the autumn, the thermocline varied significantly due to winds. The flow differed at the surface and thermoclines so that migration behaviors influenced larval retention. However, these extensive suites of swimming behaviors have never been captured in a model to date. In the past, the larvae were treated as particles with a random walk (e.g., Stewart and Arnold, 1994; Tian et al., 2009a) or simple thermocline seeking behavior (Davis et al., 2014, 2015; Gilbert et al., 2010; Munroe et al., 2018). Swimming behaviors could contribute significantly to the overall larval transport potential since they are always responding to the stimuli by changing their depth (Gallager et al., 1996). Late-stage pediveligers ( $>40$  days) migrate downwards to settle on the seabed ( $1.7 \text{ mm s}^{-1}$ ), but may remain at the thermocline for  $>100$  days and delay metamorphosis if thermal conditions are not suitable (Pearce et al., 1996). Such a delay in the settlement could lead to higher retention if larvae are in a gyre circulation. Mortality throughout the pelagic phase is carefully parameterized based on data and conditions provided in the literature (e.g., Gallager and Mann, 1986, Gallager et al., 1986, Gallager, 1988; McGarvey et al., 1992).

The Scallop-IBM consists of a super-individual tracking equation given as

$$P_i(\vec{x}_{n+1}, t_{n+1}) = P_i(\vec{x}_n, t_n) + \int_{t_n}^{t_{n+1}} \vec{\nabla}(\vec{x}, t) dt + W_b(x, y, t_n) \Delta t + R_H + R_K \quad (1)$$

where  $P_i(\vec{x}, t)$  is the egg or larval number in the  $i$ th super-individual at the location  $\vec{x} = x\vec{i} + y\vec{j} + z\vec{k}$  at the time  $t$ ;  $x$ ,  $y$ , and  $z$  are the east, north and vertical axes of the Cartesian coordinates;  $\vec{i}$ ,  $\vec{j}$ , and  $\vec{k}$  are unit vectors in  $x$ ,  $y$  and  $z$  directions; subscript  $n$  represents the  $n$ th time step;  $\vec{\nabla}$  is the three-dimensional velocity vector;  $\Delta t$  is the time step equaling  $t_{n+1} - t_n$ ;  $W_b$  is the vertical migration speed due to larval behavior;  $R_H$  and  $R_K$  are the horizontal and vertical random walks as functions of model-produced horizontal and vertical diffusion coefficients. The formulations of  $R_H$  and  $R_K$  were described in Tian et al. (2009c). Eq. (1) is solved by the 4th-order, 4-stage explicit Runge-Kutta (ERK) method with the detail given in the FVCOM User Manual (Chen et al., 2013b). The time step used in larval tracking was 120 sec, with the random walk time step of 6 sec.

The super-individual approach is commonly used in larval transport studies (Scheffer et al., 1995; Bartsch and Coombs, 2004; Woods, 2005; Tian et al., 2009a), which has a similar meaning as the simulated larvae defined in North et al. (2018). A super-individual was defined as an ensemble particle containing a total of  $1.0 \times 10^8$  individual eggs. In the Scallop-IBM, the spawning undergoes two phases before and after larval release (Tian et al., 2009c), and the larval numbers in each super-



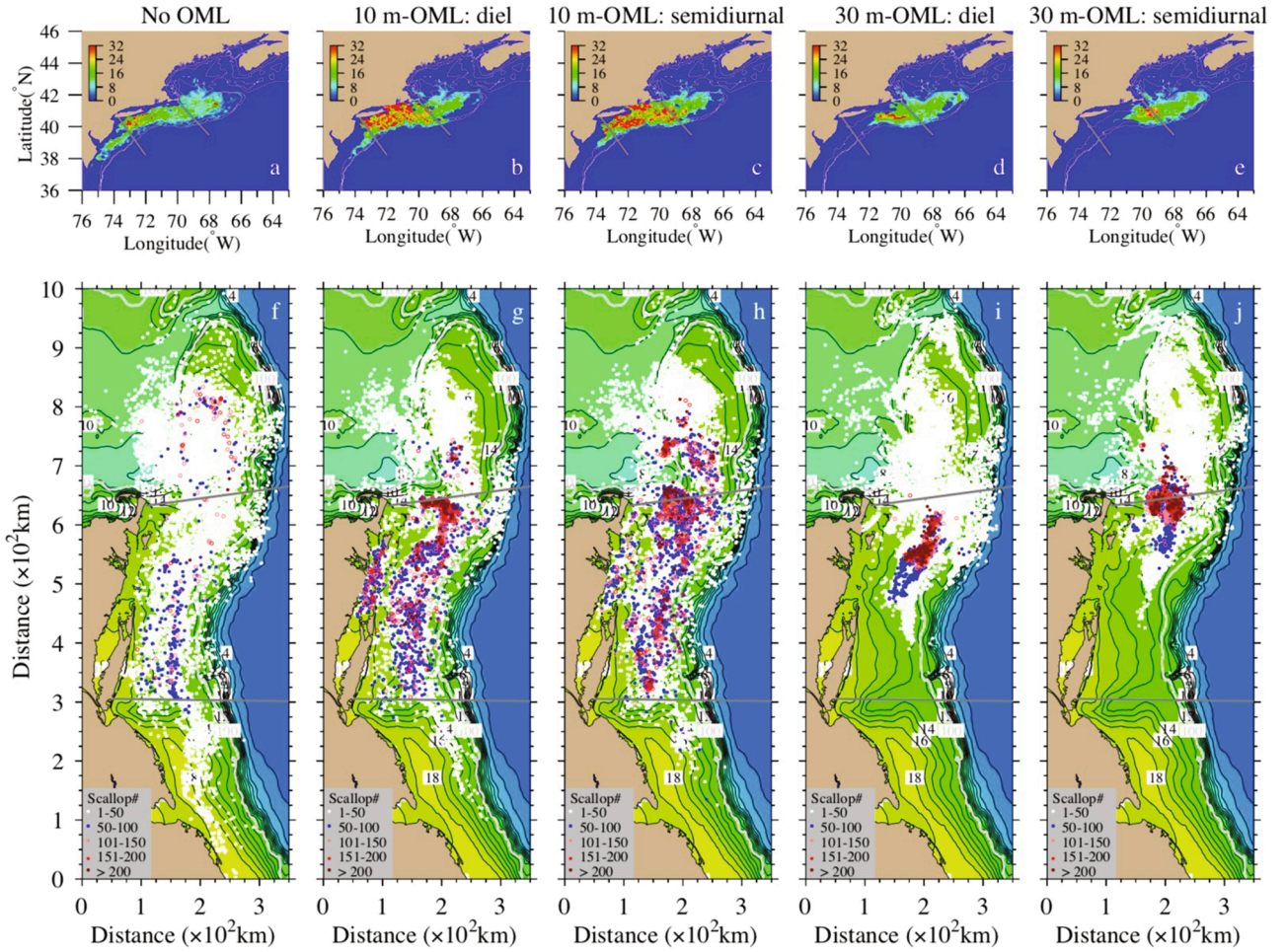


**Fig. 9.** Distributions of the settled larval density (a-e) and locations/ abundances of settled super-individuals (f-j) for the cases C#1 (No OML), C#2 (10 m-OML: diel), C#3 (10 m-OML: semidiurnal), C#4 (30 m-OML: diel), and C#5 (30 m-OML: semidiurnal). The results were from the 2012 simulation. Two thick gray lines are the boundaries between GB/GSC, SNE, and MAB. Gray lines with labels are 50, 100, and 200-m isobath contours.

individual are given as

$$P_i(\vec{x}, t) = \begin{cases} N_s E_s \int_{t_0}^t \frac{1}{\sqrt{2\pi}\sigma} e^{-\frac{1}{2}(\frac{t-t_m}{\sigma})^2} dt & \text{Spawning period} \\ P_i(n, t - \Delta t) e^{-Mt} & \text{Release period} \end{cases} \quad (2)$$

where  $N_s$  is the total adult scallops in a spawning cell at  $\vec{x}$ ;  $E_s$  is the total eggs spawned by an individual scallop;  $t_0$  is the initial time at which the  $i$ th super-individual forms;  $t_m$  is the maximum spawning time;  $\sigma$  is the standard deviation;  $\Delta t$  is the numerical integration time step.  $M$  is the instantaneous mortality rate given as a constant of  $0.25 \text{ d}^{-1}$ . This constant number was adopted from McGarvey et al. (1992) and Tian et al. (2009c). A super-individual formed as total spawned eggs reached  $1.0 \times 10^8$ . The super-individual approach helps us reduce the requirement for a computer's memory to handle a large number of particles.

### 2.3. Data

We obtained the sea scallop biomass and distribution data in the study region over 1979–2017. The data were from three sources: (1) SMAST/UMASSD, (2) U.S. NOAA, and (3) Bedford Institution of Oceanography (BIO). The SMAST/UMASSD drop camera data covered 2003–2017, NOAA dredge survey data covered 1979–2017, and BIO dredge survey data covered 2003–2017. The BIO data covered the survey areas on the eastern flank of GB in Canadian waters. We received

these data from the Bedford Institute of Oceanography (BIO), Population Ecology Division (PED), Department of Fisheries and Oceans (DFO), Canada.

### 2.4. Design of numerical experiments

We have conducted a set of the coupled scallop-IBM/NECOFS model experiments to examine (1) how sensitive the dispersal and settlement of scallop larvae are to the parameterizations of scallop larval behavior in the early stages, (2) how the interannual variability of the subtidal circulation can influence the settlement of scallop larvae, and (3) what are the physical processes affecting the larval connectivity between GB/GSC and MAB. The simulation covered the period 1978–2016. Physical variables and parameters include the flow-induced advection, water temperature, mixing intensity, and OML depth. To distinguish the physical and biological impacts, we drove the Scallop-IBM by spawning based on the multiyear-averaged abundance and distribution of adult sea scallops over 1979–2017 (Fig. 5). The scallop data used to create the multiyear-averaged field included video and dredge surveys from SMAST/UMASSD, NOAA, and BIO/Canada. Different efficiency estimates were made for video and dredge data.

Adult sea scallops spawn in the spring and fall seasons, with the dominant spawning in the autumn (Posgay and Norman, 1958). Here we only consider the fall spawning season. Following the previous approach used in Tian et al. (2009a), in each year, we specified the scallop spawning to satisfy a normal distribution starting at 00:00 GMT,



September 1 and ending at 24:00 GMT, October 10 (Fig. 6). Peak spawning was set on September 20, with a 1-week standard deviation. The major spawning, which accounted for an amount of 95% of the total spawning, was completed over four weeks, a spawning time range observed in the field measurements (Posgay and Norman, 1958; Posgay, 1976; Mullen and Morning, 1986; DiBacco et al., 1995).

The simulation was repeated yearly. Each year, Scallop-IBM was integrated over three months from September 1 to November 30, considering a time scale of ~40 days for larval settlement. Two types of experiments were made (hereafter referred to as “Exp-I and Exp-II”). For Exp-I, the model parameters were the same as those used in Tian et al. (2009a). Active vertical migration was specified for each life stage. At the age of 2 days, the larvae started migrating upward towards the surface at a speed of 0.3 mm/s. At the age of 5 days or later, the rate of upward larval migration was decreased to 0.1 mm/s. At the age of 40 days, veligers developed into pediveligers, which actively migrated downwards to the seabed at a speed of 1.7 mm/s and settled on a suitable substrate. For Exp-II, in addition to the parameters considered in Exp-I, we included the vertical migration of scallop larvae during early stages within the surface OML following the schematic patterns shown in Fig. 4. Once larvae entered the OML, the upward larval migration speed was replaced by larval vertical migration behaviors specified in the OML in all Exp-II cases. During the spawning period in September, the water was generally well mixed in the shallow regions (<40 m) over GB and stratified in the deeper water between tidal mixing and shelf-break fronts (~40–100 m) on the southern flank of GB. During that

period, the wind-induced surface OML could deepen to ~20–40 m in the stratified region. We included a vertical larval migration in the model to examine how this type of larval behavior may affect larval settlement after 40 days.

The numerical experiments were done for eight cases (Table 1). C#1 is defined as the case for Exp-I in which vertical migrations in the OML were not included. Exp-II was made for seven cases. C#2, C#3, C#4, and C#5 are defined as the cases with diel or semidiurnal vertical migration behavior in a fixed 10 or 30-m depth OML, respectively. C#6 and C#7 refer to the cases with diel and semidiurnal vertical migration behaviors in the physical model’s predicted, spatiotemporally-varying OML. We also did an experiment by constraining larvae at the bottom of the model-predicted OML after they migrated upward to the surface at the age of 5 days, and referred it to as a “thermocline-seeking behavior” case (C#8). For C#6, C#7, and C#8, the hourly OML depth was determined by vertical profiles of the model-simulated water density through an empirical method described in Appendix A. The calculated OML depth was validated via modeled temperature, salinity, and density profiles, with examples shown in Figs. A1–A4.

### 3. Influences of the surface OML on larval dispersal

#### 3.1. Comparisons between the cases with and without constant thickness OMLs

The results indicate that the dispersal and settlement of scallop

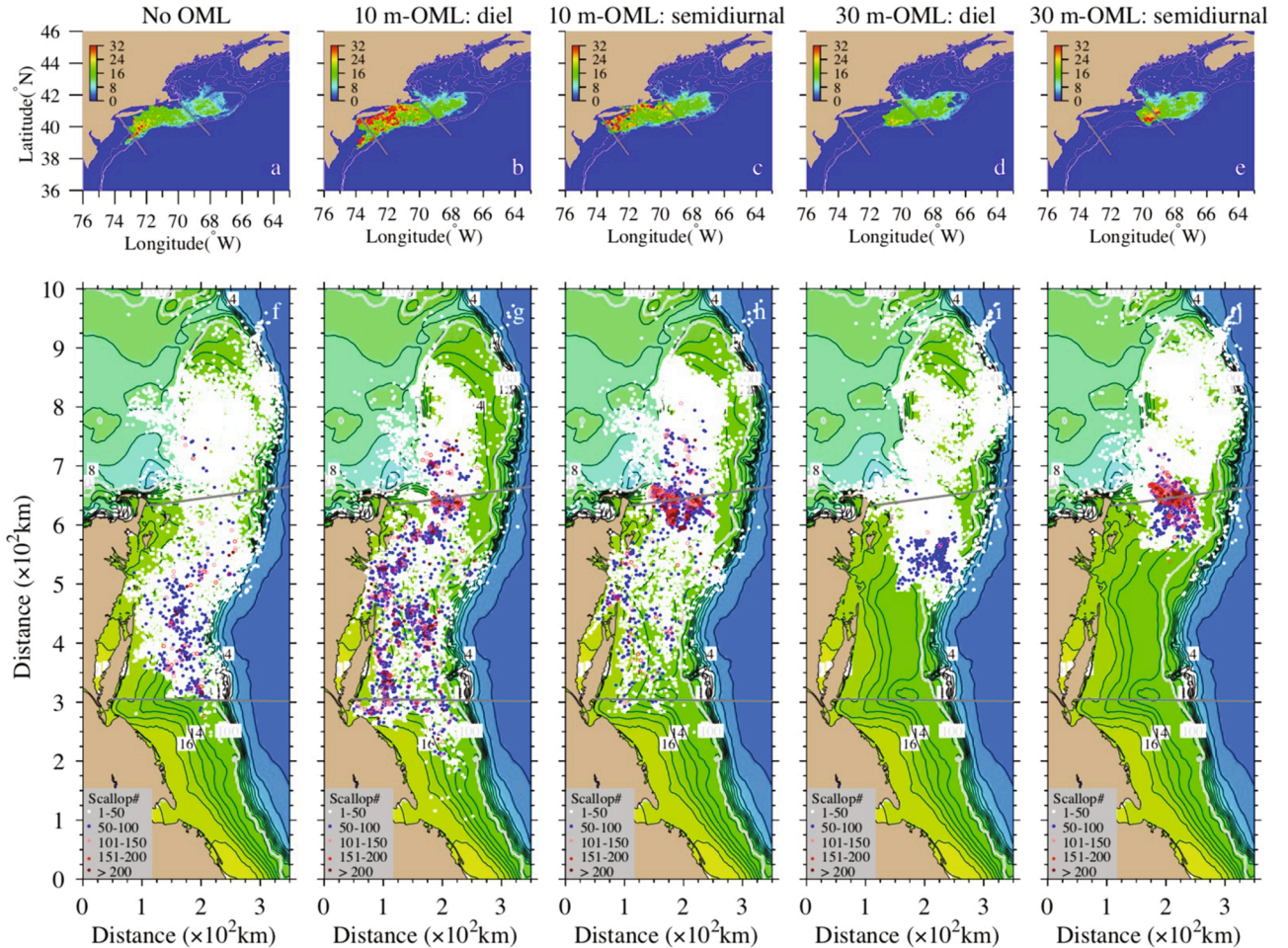


**Fig. 10.** Distributions of the settled larval density (a-e) and locations/ abundances of settled super-individuals (f-j) for the cases C#1 (No OML), C#2 (10 m-OML: diel), C#3 (10 m-OML: semidiurnal), C#4 (30 m-OML: diel), and C#5 (30 m-OML: semidiurnal). The results were from the 2013 simulation. Two thick gray lines are the boundaries between GB/GSC, SNE, and MAB. Gray lines with labels are 50, 100, and 200-m isobath contours.

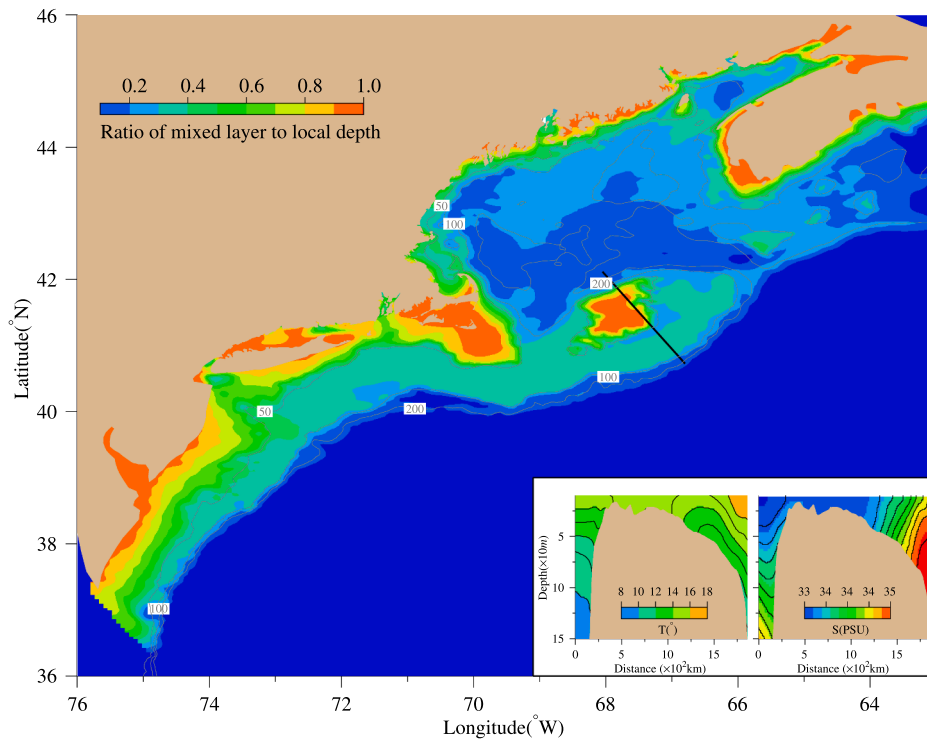


**Fig. 11.** Ratio of the model-simulated mixed layer to the local depth averaging over September–November 2013. The right lower panel shows the cross-isobath distributions of temperature and salinity on GB. The solid black thick line is the location of the section. Black lines are 50, 100, and 200-m isobath contours.

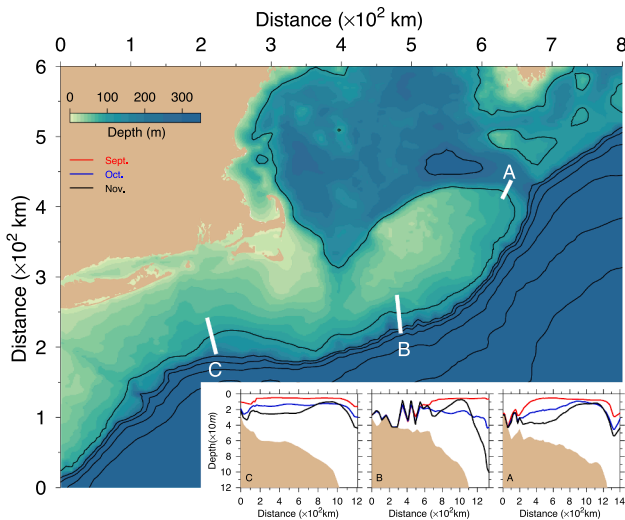


**Fig. 12.** Cross-isobath sections (thick white lines) labeled “A, B, and C” and the depths of the monthly averaged OML for September, October, and November 2013 on Sections A, B, and C, respectively. Red line: September, blue line: October, and black line: November. Black lines are the isobath contours matching with depth images. (For interpretation of the references to color in this figure legend, the reader is referred to the web version of this article.)

larvae varied significantly with scallop larval behaviors in their early stages and the thickness of the OML. It is elucidated from the abundance distributions of pediveliger settling at the seabed for the cases with and without diel or semidiurnal migration (C#1, C#2, C#3, C#4, and C#5). Examples are displayed here for 2008, 2009, 2012, and 2013 simulated numbers and concentrations of settled super-individual particle/larvae (Figs. 7–10). During the autumn of these four years, the top of GB and in other shallow regions was vertically well-mixed by tides. The OML depth

in the mixed areas was equal to the local water depth. In the following discussion, the positive and negative signs of the flow and transport referred to x- and y-directions in rotated figures (e.g., Figs. 7–10: lower panels).

In 2008, for C#1, the scallop larvae were all retained on GB and the SNE shelf, with about 49.1. and 50.9% settling in these two areas, respectively. The larvae were most abundant on the eastern side of GSC and the northeast flank of GB as well as inside the cold pool area (Fig. 7f). The cold pool is a relatively uniform cold water body ( $<13^{\circ}\text{C}$ ) near the bottom that persists from spring through fall over the mid and outer shelf regions (Lentz, 2017). For C#2 and C#3, for a specified 10-m OML, the diel or semidiurnal larval migration in the OML strengthened the larval retention within the clockwise residual gyre, resulting in 75.8 and 80.5% settling on GB/GSC, respectively (Fig. 7g, h). Although the difference in larval retention rates on GB/GSC for these two cases was only  $\sim 4.7\%$ , the spatial distributions of settled larvae differed considerably. For C#2, highly abundant larvae were settled on the western GB and within the GSC and the cold pool areas over the Nantucket Shoal. For C#3, in addition to these three areas, a large portion of larvae was settled down on the northern flank of GB. Without considering vertical migrations in the OML, many larvae were advected southward within the cold pool to the SNE shelf, with a southmost boundary off Long Island. When vertical migrations in the OML are taken into account, the larvae entering the SNE significantly reduced, accounting for  $\sim 24.2\%$  for the diel migration case and  $19.5\%$  for the semidiurnal migration case. In both cases, a relatively high abundance zone shifted northward and even entered the Long Island Sound.

When the OML was deepened to 30 m, the distributions of settled larvae significantly changed (Fig. 7i, j). The larvae tended to settle within tidal mixing and shelfbreak front zones. Although the settled larval number remained high around the clockwise gyre over GB, the highest larval abundance concentrated around the western and eastern shelves of GSC. The settled larval number reduced to 56.2% and 71.5% on GB/GSC and increased to 43.8% and 28.5% over the SNE shelf for C#4 and C#5, respectively. The OML deepening enhanced the larval



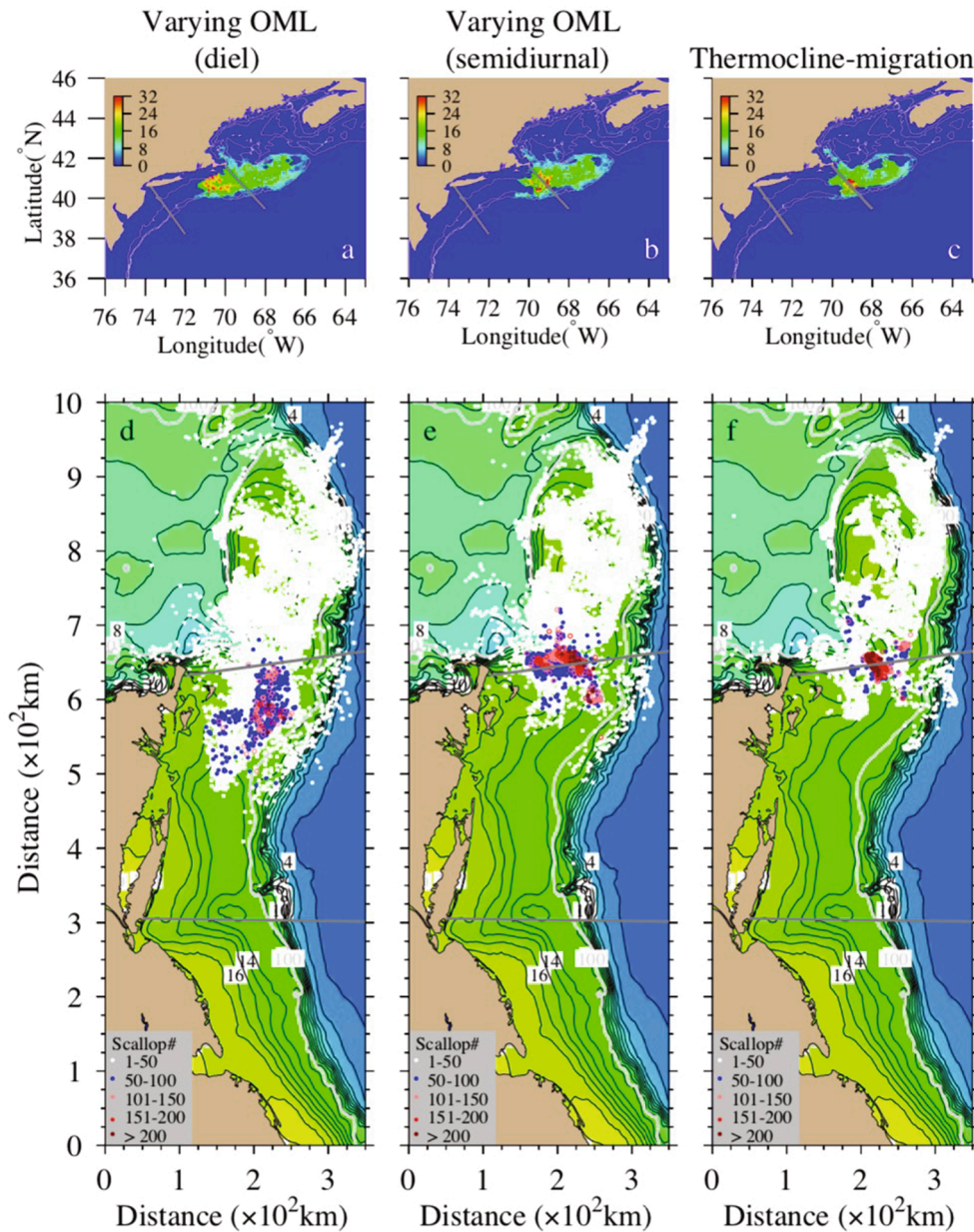


**Fig. 13.** Distributions of the settled larval density (a-c) and locations/ abundances of settled super-individuals (d-f) for the cases C#6 (varying OML: diel), C#7 (varying OML: semidiurnal), and C#8 (thermocline-migration). The results were from the 2013 simulation. Two thick gray lines are the boundaries between GB/GSC, SNE, and MAB. Gray lines with labels are the 50, 100, and 200-m isobath contours.

retention around the GSC, and restricted the southward larval transport from GB/GSC toward the MAB. In the diel migration case, the larvae over Nantucket Shoal were advected to the shelf break. That did not happen in the semidiurnal migration case. The differences shown in abundance for C#1-C#5 were observed alternatively from the larval density distributions shown in Fig. 7a-e).

The model predicts that the dispersal and settlement of scallop larvae varied significantly from year to year, which was evident in a comparison between 2009 and 2008. In 2009, regardless of larval vertical behaviors, many scallop larvae were advected to the SNE shelf and entered the MAB (Fig. 8). The main difference among C#1-C#5 was the distributions of larval settling locations, abundance, and pathways from GB/GSC to the MAB. The distributions of larval density in C#1, C#2, and C#3 were similar (Fig. 8f, g, h), except for the higher density spots occurring east of Long Island and over the MAB in C#2 and C#3. As the OML was deepened to 30 m, the larval dispersal dramatically changed.

Over GB, a large portion of larvae was settled and concentrated within the mixed area in the diel migration case (C#4) (Fig. 8i), while they expanded to cover the most area of the bank in the semidiurnal migration case (C#5) (Fig. 8j). Furthermore, the OML deepening caused larvae to shift toward the shelfbreak on their journey to the MAB. The highest larval density was found in the MAB in C#5, but not in C#4. Although significant larvae were advected southward to the MAB, the cases with larval vertical migration behaviors in the OML still provided a higher larval retention rate on GB. In C#1, 33.0% of larvae were settled over GB/GSC. The retention rate varied with the OML depth and larval behaviors. For C#2-C#4, it was increased from 39.6% to 56.2% when the OML deepened from 10 m to 30 m, while for C#5, it remained similar for the 10- and 30-m OML cases. The features described here can be viewed alternatively from the larval density distributions for C#1-C#5 shown in Fig. 8a-e.

2012 was a warm year during which the nearshore sea temperature



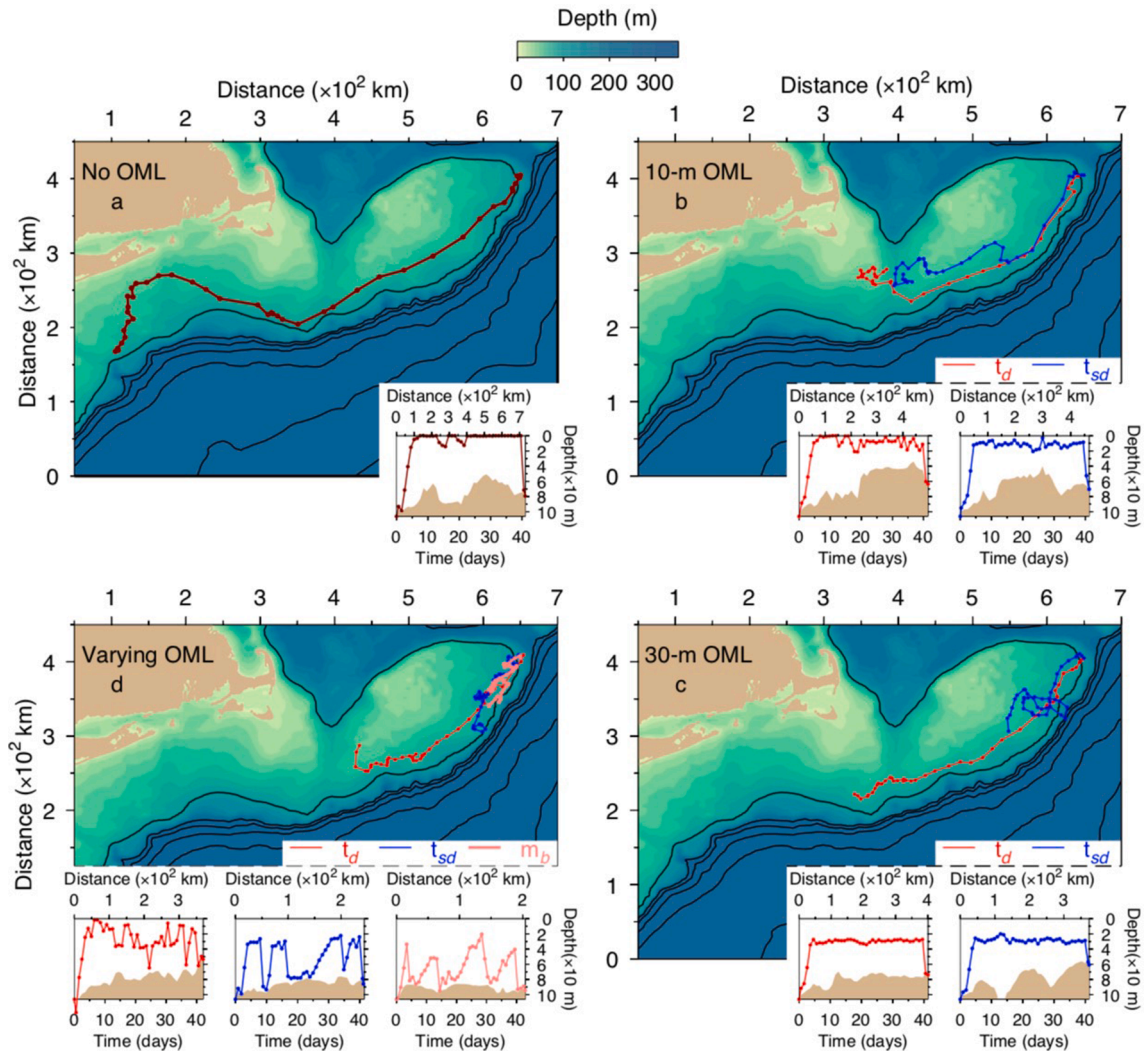


**Fig. 14.** Horizontal and vertical trajectories of a super-individual originating from the same site on the southeastern flank of GB. a: C#1 (No OML); b: C#2 and C#3 (10 m-OML); c: C#4 and C#5 (30 m-OML); d: C#6, C#7, and C#8 (Varying OML).  $t_d$ : diel;  $t_{sd}$ : semidiurnal;  $m_b$ : thermocline-seeking. The results were from the 2013 simulation. Black lines are the isobath contours matching with depth images.

increased by  $\sim 1.0$ – $2.0$  °C. Warming intensified the cross-isobath gradients of the bottom temperature over the middle shelf and shelfbreak. The settlement of larvae is influenced considerably by larval behaviors in the OML and the OML depth. For C#1, many larvae were transported to the SNE shelf and even entered the MAB, with the highest abundance over GB and within the cold pool south of Long Island (Fig. 9a, f). When diel and semidiurnal larval vertical migration behaviors were considered in a fixed 10-m depth OML (C#2 and C#3), the larvae over GB were aggregated around GSC, with a portion entering the SNE shelf (Fig. 9b, g, c, h). Although the larval distribution patterns for C#2 and C#3 were similar, the larval dispersal was more extensive in the semidiurnal migration case than in the diel migration case. As the OML depth deepened to 30 m, most larvae were retained on GB and around GSC. No larvae were advected southward to enter the MAB. For a given OML depth, the larval distributions varied with larval behaviors in the OML. For C#4, the settled larvae showed a dispersive distribution on GB, with the highest abundance in the cold pool area over Nantucket Shoal west of GSC (Fig. 9d, i). For C#5, the larvae were settled around the tidal-mixing front on GB, with a dense aggregation around GSC (Fig. 9e, j). The results for C#4 and C#5 were correlated well with the extremely high recruitment found in NLCA from 2012 (Bethoney et al., 2016).

Changes in the larval dispersal and settlement with the OML depth and larval behaviors in 2013 were similar to that found in 2012

(Fig. 10). Either ignoring larval behaviors in the OML (C#1) or having larval behaviors in a thin OML (C#2 and C#3) overestimated the southward larval transport. The deeper OML favored larval retention over GB/GSC and Nantucket Shoal (C#4 and C#5). For a given 30-m OML, the larval dispersals significantly differed for the diel (C#4) and semidiurnal (C#5) migration cases. For C#4, the highest larval aggregation area was on the SNE (Fig. 10d, i), while for C#5, it was around the GSC (Fig. 10e, j). Over GB, similar to 2012, the settled larvae were distributed on the top and western areas in the C#4 case, while they occupied the entire bank in the C#5 case.

The significant difference among C#1–C#5 for 2008, 2009, 2012, and 2013 illustrates that the larval dispersal and settlement varied not only by the changes in physical environments but also with larval behaviors in the OML. Larval behaviors in the OML made larvae stay longer in the vertical column before settling, increasing the larval residence time on GB. Thus, ignoring it will overestimate the larval transport to the SNE shelf and MAB.

### 3.2. Influences of larval behaviors in the varying-thickness OML

The OML depth varied significantly in time and space, especially during spring and autumn (Flagg, 1987). In these two seasons, it was in a range of 10–40 m over the shelf (Li et al., 2020). The vertically well-

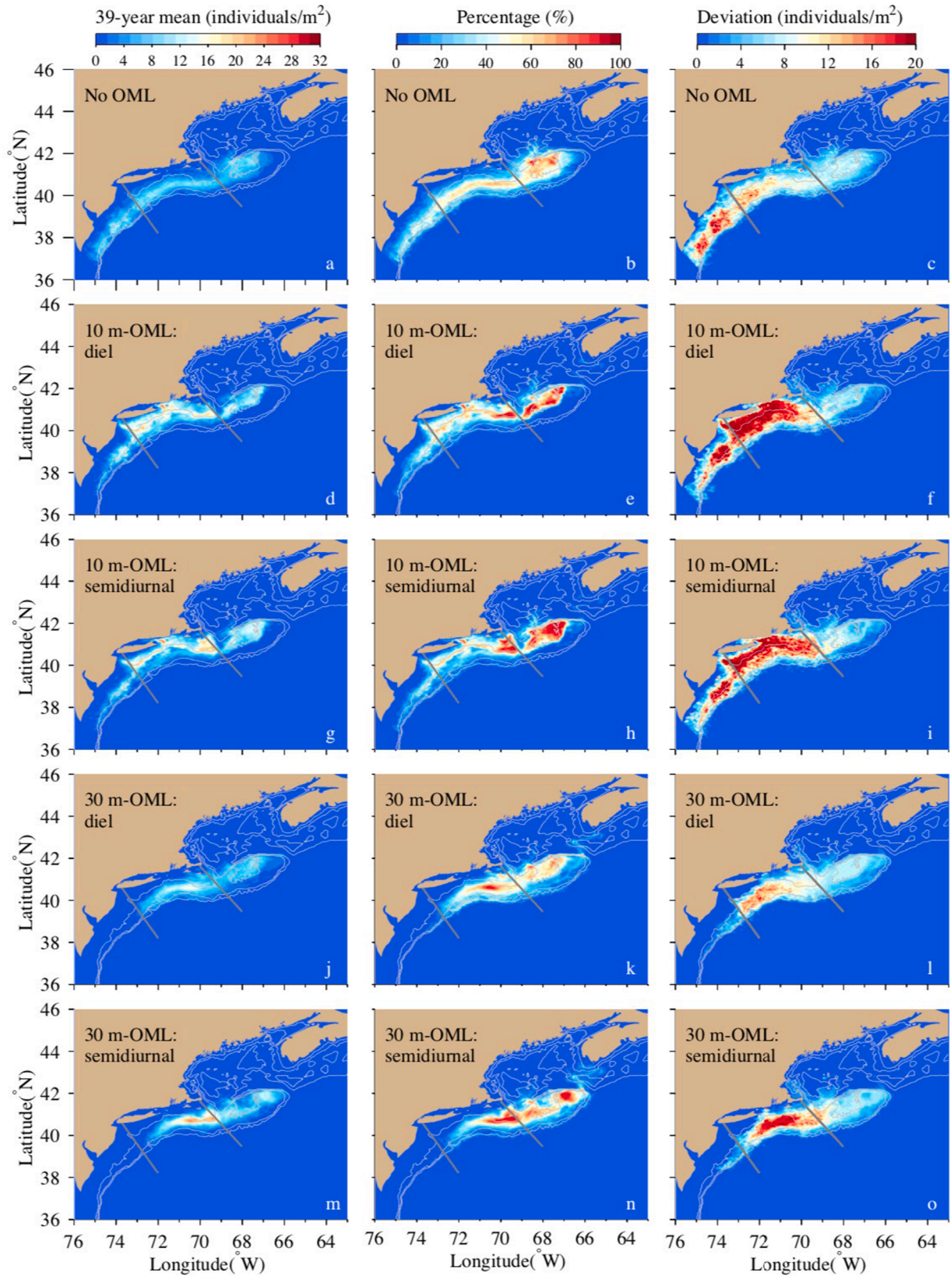


**Fig. 15.** The 39-year mean, percentage, and standard deviation of settled scallop larvae over 1978–2016 for C#1–C#5. a–c: C#1 (No OML); d–f: C#2 (10 m-OML: diel); g–i: C#3 (10 m-OML: semidiurnal); j–l: C#4 (30 m-OML: diel); m–o: C#5 (30 m-OML: semidiurnal). Two thick gray lines are the boundaries between GB/GSC, SNE, and MAB. Gray lines are the 50, 100, and 200-m isobath contours (see Fig. 11 for isobath labels).

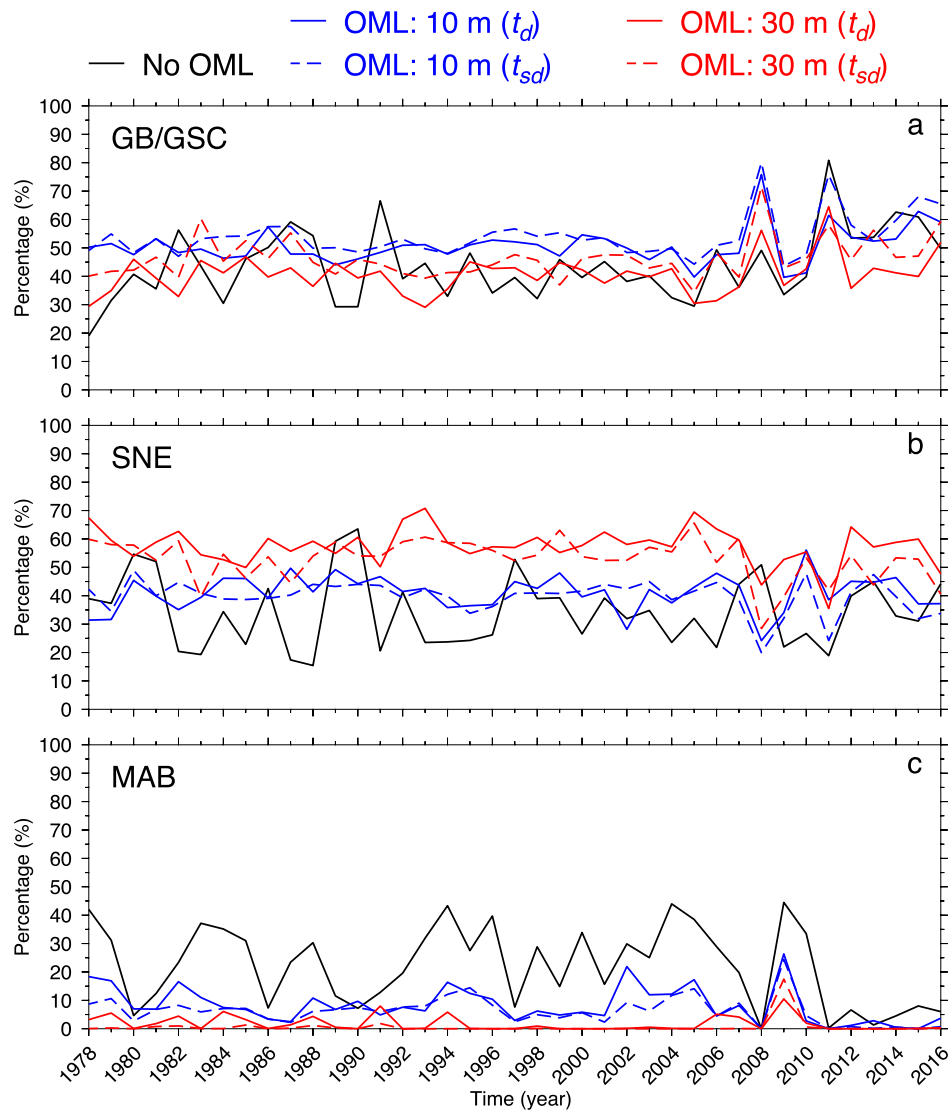


**Fig. 16.** Model-predicted percentages of the scallop larvae settling in the GB/GSC (a), SNE (b), and MAB (c) regions, respectively, over 1978–2016 for C#1 (solid black line), C#2 (solid blue line), C#3 (dashed blue line), C#4 (solid red line), and C#5 (dashed red line). (For interpretation of the references to color in this figure legend, the reader is referred to the web version of this article.)

mixed and stratified areas were distinct in the model-predicted mean water density profilers throughout September–November. In 2013, for example, the water was vertically well-mixed in areas where bottom depths were shallower than 50 m over GB and Nantucket Shoal, while it was strongly-stratified on the southern flank of GB, in GSC, and over middle/outer shelves of SNE and MAB (Fig. 11). Three sections labeled A, B, and C were selected to show the variability of the OML on the eastern and southern flanks of GB and the SNE shelf over September–November (Fig. 12). Over GB, in the areas between tidal and shelf-break fronts, the OML depth was ~10 m in September and then gradually increased to ~30–40 m or deeper in November (Fig. 12: see A and B). Within the shelfbreak front, the OML depth remained steady after October. On Section-B, the OML thinned rapidly in November, suggesting a local scale onshore intrusion of the stratified Gulf Stream water during that period. The temporal variability of the OML at Section-C over the SNE shelf was similar to that at Section-A on the eastern flank of GB.

To examine the influence of larval behaviors in a varying OML on the dispersal and settlement of scallop larvae, we repeated the 2013–2016 experiments with the real-time OML provided hourly from NECOFS (C#6 and C#7). We also ran the model with a thermocline-seeking

larval behavior in the same model-predicted OML (C#8). These additional cases were conducted over the same period, starting on September 1 and ending on November 30. The comparison was made among results obtained for eight cases (C#1–C#8) with and without the inclusion of larval behaviors.

The results showed that the variability of the OML had a marked influence on the scallop larval dispersal. An example was exhibited here for 2013 simulation results. Although the settled larval distributions were similar between C#6 (Fig. 13a, d) and C#4 (Fig. 10d, i) and also between C#7 (Fig. 13b, e) and C#5 (Fig. 10e, j), the spatiotemporal variation of the OML pushed larvae in the highly abundant area northward to the Nantucket Sound in C#6 (Fig. 13a, d) and aggregated larvae on the western shelf of GSC in C#7 (Fig. 13b, e). C#8 considered a case for constraining larvae at the bottom of the OML. In this case, most of the larvae aggregated on southern and western flanks of GB, within the region between 50- and 100-m isobaths (Fig. 13c, f). The highest larval density area was in the GSC area, but the abundance was much smaller than those found for C#7. For C#7 and C#8, either semidiurnal migration or thermocline-seeking behavior consistently predicted a larval aggregation in the closed area around GSC. This feature was not captured in the case without larval behaviors in the OML.



**Table 2**

Mean percentages and standard deviations of larvae settling in GB/GSC, SNE, and MAB over 1978–2016 for C#1–C#5.

Cases	GB/GSC	SNE	MAB
C#1: No OML	43.7 ± 12.4	34.2 ± 12.5	22.1 ± 13.9
C#2: 10-m OML: diel	50.7 ± 6.5	41.1 ± 6.3	8.2 ± 6.3
C#3: 10-m OML: semidiurnal	53.9 ± 7.5	39.8 ± 5.8	6.3 ± 4.9
C#4: 30-m OML: diel	40.7 ± 7.0	57.5 ± 6.6	1.8 ± 2.7
C#5: 30-m OML: semidiurnal	46.3 ± 7.2	53.0 ± 7.5	0.7 ± 2.8

Changes in the residence time of larvae in the water column on GB were one of the reasons for distinct differences in the larval dispersal and settlement for C#1–C#8. For example, tracking a super-individual originating from the same initial location on GB for these eight cases, we examined horizontal and vertical movements of this super-individual under different biophysical environments (Fig. 14). In each case, the tracking period was 41 days, with its trajectory sampled daily. For C#1, the super-individual migrated upward to the sea surface at the 5-day age and then stayed there until they grew to the 40-day age. The near-surface flow rapidly advected this super-individual southward along the shelf, with a residence time of ~15 days on GB (Fig. 14a). When larval behaviors in the OML were considered, the daily larval trajectory varied with the sampling method. Here sampling was taken at noon each

day. At this time, the larvae were mainly at the bottom of the OML regardless of diel, semidiurnal, and thermocline-seeking larval behaviors.

For C#2 and C#3, the super-individual migrated upward to the subsurface at a depth of 10 m at the 5-day age and moved southward following a daily mean trajectory at the bottom of the OML (Fig. 14b, c). After 40 days, it settled to the seabed around GSC. Compared with the diel migration behavior, the semi-diurnal migration behavior favored retaining the larvae on GB, even though their trajectories almost coincided during the first 7 days. As a result, the super-individual settled on the western shelf of GSC in C#2, but within the GSC in C#3 (Fig. 14b).

Similar features were also found for C#4 and C#5 when the OML depth was deepened to 30 m. In the diel vertical migration case (C#4), after the super-individual migrated upward to enter the OML, it followed a daily trajectory at the bottom of the OML to move southward along the bank (Fig. 14c). This super-individual then settled down near the shelf break of the SNE shelf. Differing from C#4, the super-individual in C#5 was trapped locally after 8 days and eventually settled around 60-m isobath area on the southern flank of GB after 40 days (Fig. 14c). For a given fixed-depth OML, the longer distance in vertical migration tended to make the larvae move slowly in the horizontal. This feature was also observed in the spatiotemporally-varying OML cases, even though horizontal and vertical trajectories of the super-individual significantly differed.

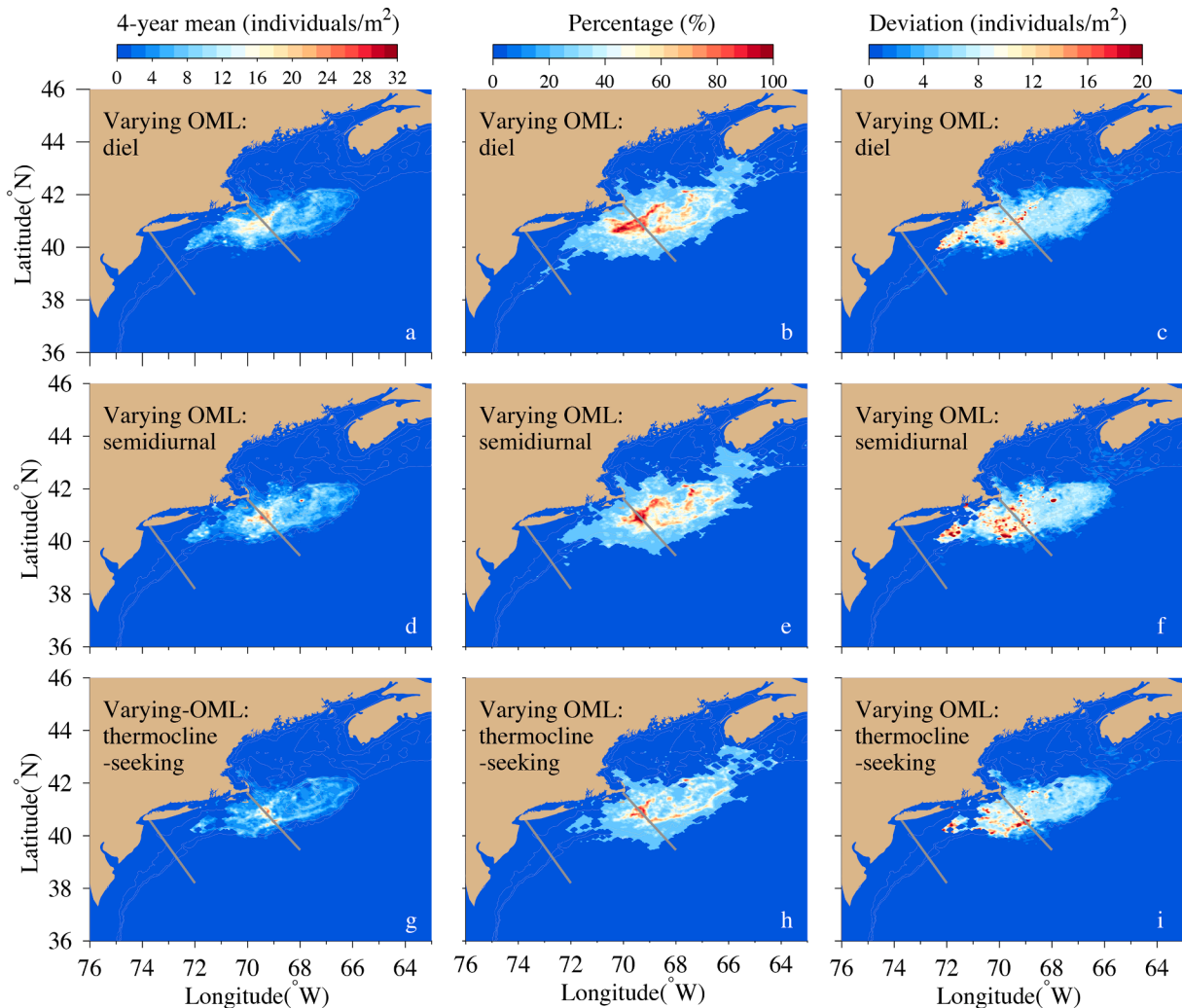


**Fig. 17.** The 4-year mean, percentage, and standard deviation of settled scallop larvae over 2013–2016 for C#6, C#7, and C#8. a–c: C#6 (varying OML: diel); d–f: C#7 (varying OML: semidiurnal); g–i: C#8 (thermocline-migration). Two thick gray lines are the boundaries between GB/GSC, SNE, and MAB. Gray lines are the 50, 100, and 200-m isobath contours (see Fig. 11 for isobath labels).

**Table 3**

Mean percentages and standard deviations of larvae settling in GB/GSC, SNE, and MAB over 2013–2016 for C#6, C#7, and C#8.

Cases	GB/GSC	SNE	MAB
C#6: Varying OML: diel	53.5 ± 7.0	46.5 ± 7.1	0.0 ± 0.1
C#7: Varying OML: semidiurnal	57.7 ± 6.1	42.5 ± 6.1	0.0 ± 0.0
C#8: Varying OML: thermocline-seeking	62.9 ± 8.8	37.1 ± 8.8	0.0 ± 0.0

The diel vertical migration behavior (C#6) was less favorable to retain the larvae on GB compared with semidiurnal (C#7) and thermocline-seeking (C#8) vertical migration behaviors (Fig. 14d). For C#6, the super-individual followed the clockwise gyre circulation to drift along the bank during the first 35 days, then turned northward on the western GB, and eventually settled at the seabed east of the GSC. The trajectory of this super-individual varied significantly in the vertical before settling. For C#7 and C#8, the semidiurnal or thermocline-seeking vertical migration pushed the super-particle offshore toward the shelfbreak front, retained it in the deeper depth, and eventually made it settle on the southeastern flank of GB, an area close to its origin. In these two cases, the thermocline-seeking behavior was more favorable to restrain the horizontal movement than the semidiurnal behavior. It explains why similar aggregation patterns were found for C#7 and C#8 around the GSC. The comparison of horizontal and vertical trajectories of the same super-individual in these eight cases again highlights the importance of including larval behaviors in the OML in the Scallop-IBM, especially for the early life stage simulation.

### 3.3. Statistics and connectivity of scallop larvae over GB/GSC, SNE, and the MAB

Dividing the model domain into  $2 \times 2$  km boxes, we statistically calculated the mean, percentage, and standard deviation of larval density over 39 years from 1978 to 2016 for C#1–C#5, respectively. Probability is represented by the settling percentage of larvae in each box over 39 years, ranging from 0 (0%) to 1 (100%). Standard deviation was estimated relative to the 39-year mean, which illuminated the range of the interannual variability. For C#1, the mean larval density remained high over GB/GSC and SNE, with a significant interannual variability occurring in the SNE and MAB region (Fig. 15a–c). In this case, the probability rate of larvae entering the MAB was up to 50%. For C#2 and

C#3, the diel vertical larval migration tended to retain larvae over GB/GSC and SNE, with maximum interannual variability occurring over the SNE shelf and northern area of the MAB (Fig. 15d–i). In these two cases, the model showed that including the larval behavior in the OML considerably reduced the probability rate of larvae entering the MAB. The major difference between these two cases was in the spatial distribution of settled larvae over GB/GSC and SNE. In the semidiurnal case, more larvae accumulated in the eastern portion of NLCA and the center of GB. For C#4 and C#5, deepening of the OML favored the larval retention over GB/GSC and SNE and restricted larval transport from entering the MAB, even though it happened occasionally (Fig. 15j–o). Similar to the 10-m OML case, the primary difference between diel and semidiurnal migration cases was in the spatial distribution of settled larvae. The semidiurnal migration behavior in the OML led to denser larval accumulation in the three closed areas, especially in the northern portion of CA-II over the northeastern flank of GB. Regardless of whether larval swimming behaviors in the OML were considered, the SNE was a region featuring the maximum larval interannual variability.

We estimated the percentage of larvae settling in three geographic zones of GB/GSC, SNE, and the MAB (see the boundary of each zone in Fig. 1) for C#1–C#5, respectively. The model consistently predicted that GB/GSC was a high retention area (Fig. 16 and Table 2). C#2 and C#3, also C#4 and C#5, exhibited a similar interannual variability pattern. On GB/GSC, the mean differences over 1978–2016 were 7.0% between C#2 and C#1, and up to 10.2 between C#3 and C#1, indicating that the semidiurnal migration behavior increased the retention by  $\sim 3.2\%$  (Fig. 16a). When the OML depth was deepened to 30 m, the retention rate on GB/GSC was decreased by 3.7% for the diel migration case and 7.0% for the semidiurnal migration case. The SNE shelf was also a high aggregation area of scallop larvae (Fig. 16b). In this region, considering larval behaviors in the OML increased the larval settlement rate. The rate became higher as the OML deepened. The 39-year mean difference was 6.9% between C#2 and C#1, and 5.6% between C#3 and C#1. The difference was up to 23.3% between C#4 and C#1, and 18.8% between C#5 and C#1.

The most considerable difference among C#1, C#2, C#3, C#4, and C#5 was the larval settlement rate in the MAB. For C#1, the model predicted a sizeable larval transport to the MAB, with a 39-year mean of 22.1% and a maximum of up to 40% (Fig. 16c). The larval transport to the MAB was considerably reduced by taking larval behaviors in the OML into account. Except for 2009, it was about 10% or less than for

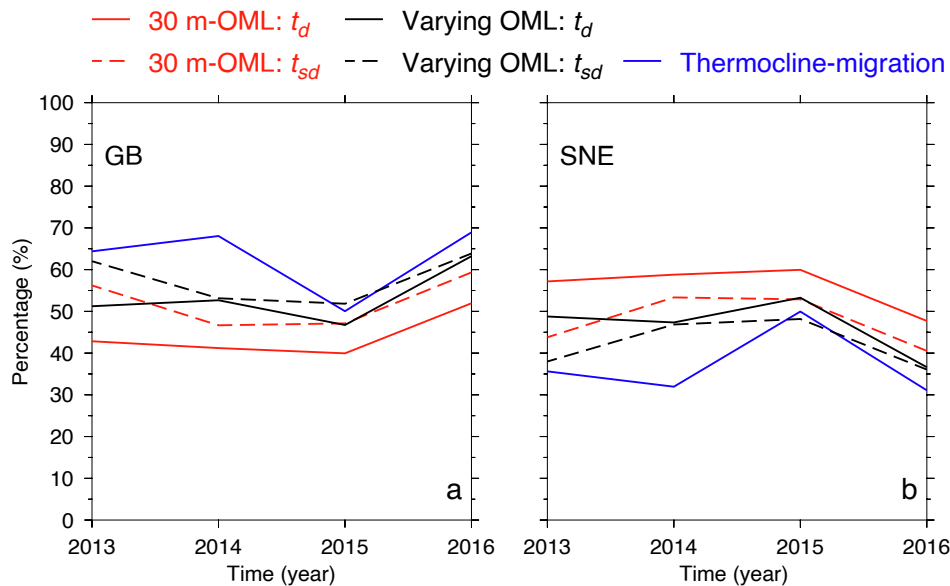


**Fig. 18.** Model-predicted percentages of the scallop larvae settling in the GB/GSC (a) and SNE (b) regions, respectively, over 2013–2016 for the cases C#4 (30 m-OML: diel), C#5 (30 m-OML: semidiurnal), C#6 (varying OML: diel), C#7 (varying OML: semidiurnal), and C#8 (thermocline-migration).

C#2 and C#3, 5% or less for C#4, and close to zero for C#5. The 39-year means for C#2-C#5 were 8.2, 6.3, 1.8, and 0.7%, respectively. These results suggest that the GB/GSC and MAB scallop populations were poorly connected by larval transport. The high scallop abundance observed in the MAB might have been produced by a high recruitment rate of larvae spawned in the local region.

We started implementing a method to determine the real-time OML depth in the simulation in 2013. The experiments for varying OML were done for 2013–2016. The statistics of these four-year results for C#6-C#8 showed that regardless of vertical migration patterns, the GB/GSC and SNE had high scallop larval settlement, with the maximum interannual variability occurring over the SNE shelf (Fig. 17, Table 3). In particular, the spatiotemporal variability of the OML led to denser larval accumulation in the NLCA. No larvae were advected into the MAB in all three cases of C#6, C#7, and C#8. We also estimated the percentage of larvae settling in three geographic zones of GB/GSC, SNE, and the MAB for these three cases and compared the results with C#5. For the semi-diurnal migration case, the interannual variability for C#5 and C#7 exhibited a similar pattern in the GB/GSC and SNE regions (Fig. 18). The spatiotemporally-varying OML produced a high retention rate on GB/GSC, with a 5.4% difference between GB/CSC and SNE regions for these two cases. Also, C#7 predicted less larval transport to the MAB than C#5, even the transports for both cases were close to zero. For the diel migration case, although the settled larvae percentages in the GB/GSC and SNE regions showed a similar variation for C#6 and C#4, the spatiotemporally-varying OML produced a more favorable condition to retain the larvae on GB/GSC than the fixed-depth OML. The difference was up to 9.5% between GB/GSC and SNE regions for these two cases. The larval settlement showed relatively large variability in C#8. The mean percentages over 2013–2016 were 62.9% over GB/GSC, 37.2% over the SNE shelf, and 0.0% entering the MAB.

#### 4. Discussion

Our results indicate that the larval vertical migration in the OML can significantly influence the dispersal and settlement of scallop larvae over GB/GSC and SNE, as well as larval transport to the MAB. In the GB/GSC and SNE regions, although the 39-year mean difference was in the range of ~10% or less between C#1 and C#2-C#5, their dispersal patterns

differed considerably. Vertical migration made scallop larvae stay longer in the water column on GB/GSC as compared to passive larvae, because it exposed them to different currents in the deeper water, which were slower and more cyclonic (Werner et al., 1993; Page et al., 1999). As a result, the larvae originating from eggs spawned on GB, mainly drifted around the bank following the clockwise residual flow and eventually settled on GB and surrounding SNE areas. Only a few moved southwards to enter the MAB.

The conclusions in Tian et al. (2009a, 2009c) were similar to our findings for C#1 (without swimming behaviors) but very different from the results for C#2-C#8 (swimming that oscillated between subsurface depths). We believe that the difference was due to the physics and larval behaviors. Tian et al.'s (2009a, 2009b, 2009c) simulations did not include the Gulf Stream-shelf interaction and inflow from the upstream Labrador Sea and the Arctic Ocean. The currents used to drive the Scallop-IBM significantly differed from the NECOFS fields used in this study, especially at the shelf break where the Gulf Stream influences were significant. Tian et al. (2009c) implemented a thermocline-seeking larval behavior in the Scallop-IBM. They assumed that the OML depth remained constant, with thermoclines always at a depth of 23 m. Once larvae migrated to 23 m, they drifted as passive particles along with the horizontal flow at that depth. The simulation covered 1995–2005, and the results showed significant larval transport to the MAB in 1998, 2001, 2004, and 2005. Especially in 2005, the larval settlement in the MAB was even more than larvae settled over GB/GSC. Comparing our simulation results with Tian et al. (2009a, 2009c) for the same period 1995–2005, we found that no matter how the OML depth was specified, the models predicted a high aggregation over GB/GSC and SNE, and a weak connection between GB/GSC and the MAB. Even in 2005, the larval transport to the MAB was only around 10% for C#2 and C#3 and close or equal to zero for C#4 and C#5. Over 2013–2016, we repeated the thermocline-seeking larval behavior experiment (C#8) with a similar approach used in Tian et al. (2009c), but we considered the spatiotemporal variation of the OML depth (Fig. 17). In this case, larval transport to the MAB was non-existent.

Tian et al. (2009c) argued that vertical migration played a less critical role in the dispersal and settlement of scallop larvae originating from GB/GSC. Their argument was based on two pieces of evidence observed by Gallager et al. (1996) and Tremblay and Sinclair (1990a).

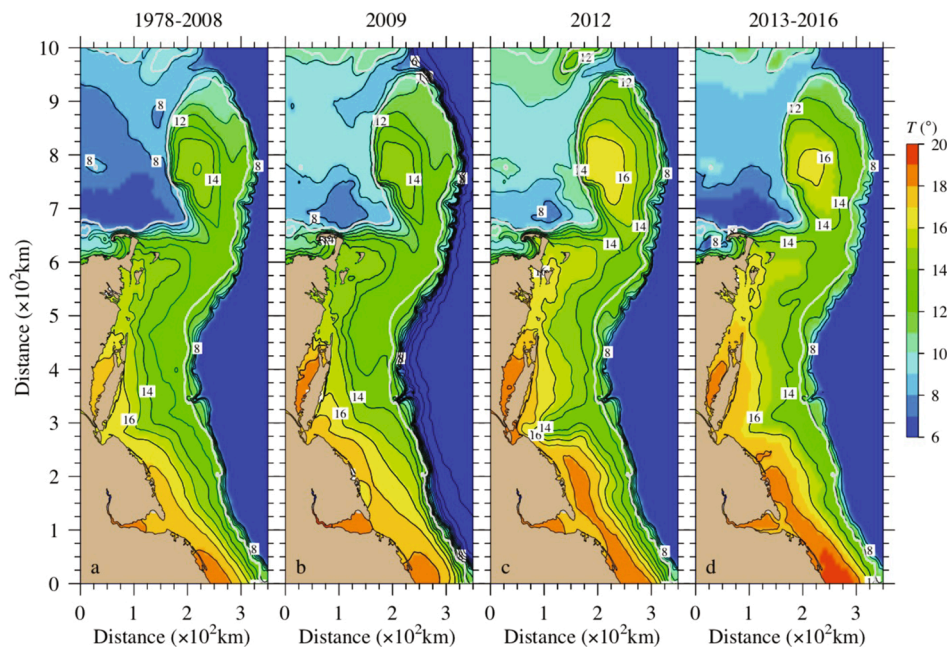


Fig. 19. Distributions of the three-monthly averaged bottom temperature in the region covering GB, SNE, and the MAB over September–November. a: 1978–2008-averaged; b: 2009; c: 2012; d: 2013–2016 averaged.



Gallager et al. (1996) detected the larvae migration in the OML, aggregating twice at the sea surface during the night and at the bottom of the OML during the day (e.g., Fig. 4). The measurements were made in a thin OML of  $\sim 4$  m (mesocosm). Tian et al. (2009c) assumed that such a short-distance vertical migration would not affect the larval dispersal since the horizontal drifting velocity zone or the residence time remained unchanged. The fact was that the OML depth varied significantly in autumn, especially during a storm event (Li et al., 2020). Tremblay and Sinclair's profiler sampling showed a high larval abundance within thermoclines at depths varying in the range of 12–23 m on GB. Based on this observation, Tian et al. (2009c) questioned whether active larval vertical migration was a general feature on GB. The profiler sampling was done at different times, and each was completed in 74 min. A few in-situ observations were not sufficient to cover the daily migration period. Small amplitude diel vertical migration was also found in a shallow area of  $< 25$  m off Grand Mann Island in the Gulf of Maine by Tremblay and Sinclair (1990b). Therefore, it may have been premature to conclude that no vertical migration of larvae existed in the region.

The scallop larval dispersal and settlement results for cases with semidiurnal and thermocline-seeking migrations (C#7 and C#8) suggest that there was almost no larval connectivity between GB/GSC and the MAB. Although the larval distributions for these two cases differed and the settlements showed more considerable variability in C#8 than in C#7, the 4-year mean settled larval percentages in either GB/GSC or SNE regions were 5.4% or less for these two cases.

Our simulation results with larval migrations within the OML show that 2009 was a year with a significant larval transport from GB/GSC to the MAB. Since that year, the retention rate of migrating larvae in the GB/GSC and SNE regions remained a high value, with almost no larvae transporting southward into the MAB. The bottom temperature over the northeast shelf was characterized by a cold pool, forming in spring, and gradually decaying through autumn (Lentz et al., 2003; Lentz, 2017). Although this cold pool's intensity was considerably weak in autumn, it was still visible as a relatively uniform cold temperature region bounded by  $12$ – $13$  °C contours in Fig. 19. Compared with the climatological mean bottom temperature over 1978–2008 (Fig. 19a), in 2009, the cold pool area expanded onshore over the SNE shelf and shrank towards the shelfbreak south of Long Island (Fig. 19b). 2012 was a warm year with a  $\sim 2$  °C rise of the bottom temperature in the tidally well-mixed area of GB and nearshore regions (Fig. 19c). Warming significantly shrank the area of the cold pool and pushed it offshore. The well-defined cold pool disappeared on the southern flank of GB due to the warming-induced intensification of the cross-isobath gradient of bottom temperature. This feature was sustained over 2013–2016 (Fig. 19d). The cold pool functioned as an index for the GB/GSC, SNE, and MAB connectivity. The weakening of the cold pool's intensity and intensified cross-isobath gradient of bottom temperature tends to enhance the clockwise gyre circulation over GB, which indirectly supported our finding: warming has restricted the larval transport from GB/GSC to the MAB.

The warming tendency was evident in the satellite-derived sea surface temperature (SST) change over the U.S. northeastern shelf in the past decades (Fig. 20). Significant warming occurred in 2012. After that, the water remained warmer. The yearly warming rate of the SST averaged over the shelf bounded at the 300-m isobath was  $\sim 0.04$  over 1982–2020 (Fig. 20a). Assuming 2012 as a year for warming regime shift, the mean SST after that was about  $1.0$  °C higher than the climatological SST mean averaged over 1982–2011. This warming feature was captured in the NECOFS simulation. The warming rate in the region varied significantly in space, with the maximum around the shelfbreak off GB (Fig. 20b). We examined the NECOFS-predicted subtidal flow field in the region and found a branch of the Gulf Stream that flowed northeastward towards GB. This branch flow has been intensified significantly in recent years, causing extreme warming at the shelfbreak off GB. As we detected in the NECOFS-simulated temperature and flow fields, the warming has intensified the cross-isobath gradient of water

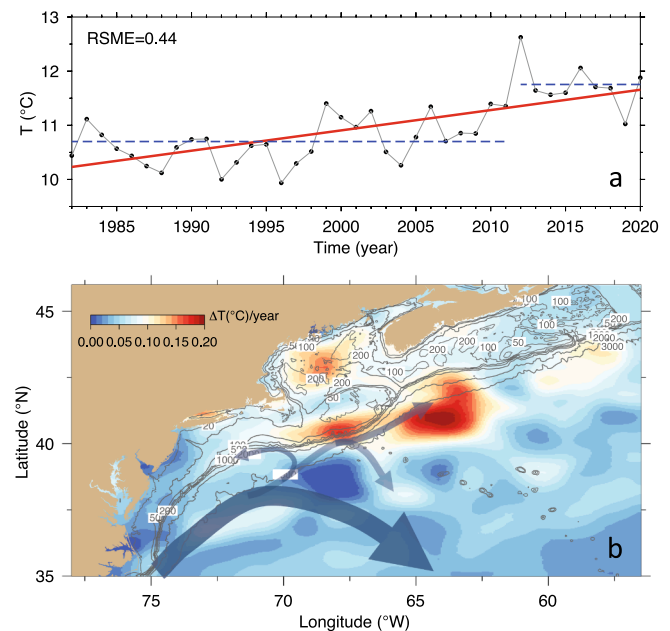


Fig. 20. b: distribution of the yearly surface temperature increase rate calculated based on the satellite-derived SST data over 1982–2020. The temperature increase rate was estimated based on the annual increase rate calculating over two consecutive years. a: the change of the satellite-derived SST over the shelf bounded by the 300-m isobath over 1982–2019. Solid black dots: the yearly averaged SST for each year; thick red line: the linear regression fitting line; thick blue dashed lines: averaged SSTs over 1982–2011 and 2012–2020, respectively. (For interpretation of the references to color in this figure legend, the reader is referred to the web version of this article.)

temperature on the southern flank of GB and thus strengthened the clockwise gyre over the bank.

The model predicted extensive southward water transports in the autumn of 2009. Selecting a cross-shelf section over the SNE shelf (see the location in Fig. 1), we calculated the water transport through that section over 1978–2016. Across that transect, the 39-year mean transport was  $-0.46 \times 10^{-3}$  Sv ( $\text{Sv} = 10^6 \text{ m}^3/\text{s}$ ). The anomaly exhibited relatively large positive (northward) and negative (southward) phases in 2008 and 2009, respectively, and remained positive since 2011 (Fig. 21). The anomaly's interannual variability explains why the larval transport to the MAB was most extensive in 2009, and no connectivity between GB/GSC and the MAB had occurred since 2010. The wind was a primary driver for the sizeable southward transport in autumn of 2009. The wind records at Buoy#44008 show that differing from other years, the northeasterly wind prevailed over the northeast shelf during autumn

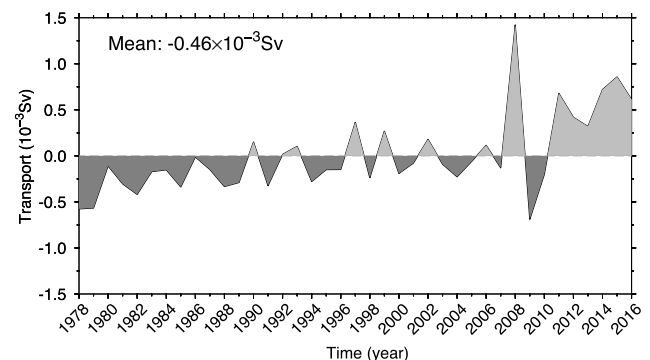


Fig. 21. Anomalies of the water transport through an across-shelf section over the SNE shelf (see the location in Fig. 1) over 1978–2016. The value listed in the upper-right area is the 39-year mean water transport.

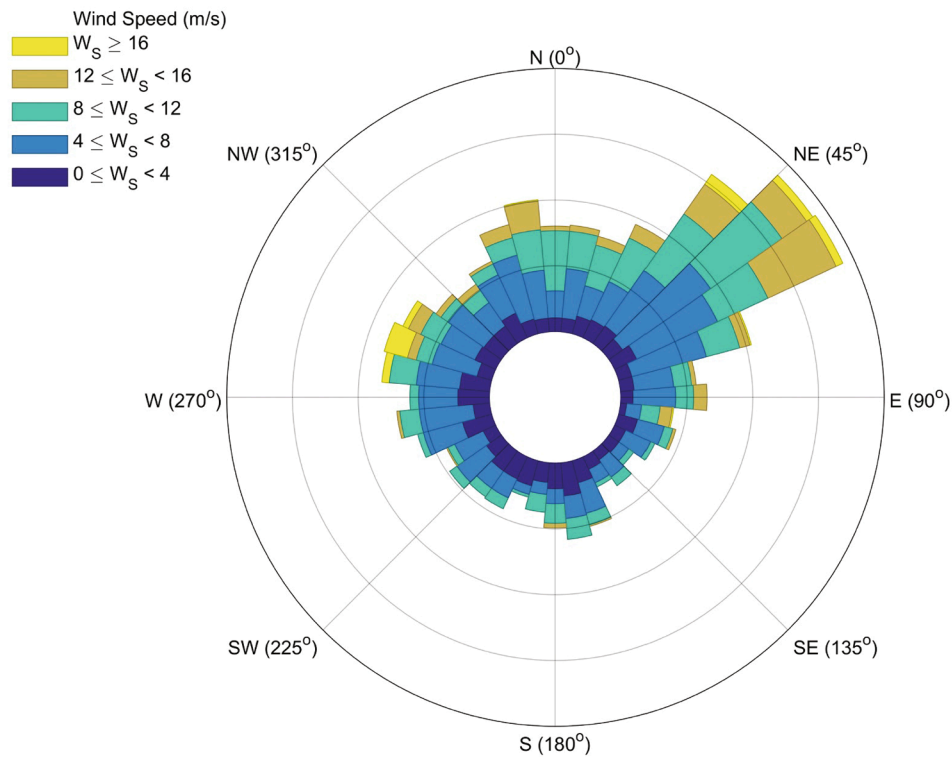


Fig. 22. The wind rose plot at NOAA buoy 44,008 for September–November 2009.

of 2009, with a maximum speed of  $>16$  m/s (Fig. 22). The extreme northeasterly or northerly winds tended to push the water onshore. It enhanced the southward along-shelf flow under a balance between the pressure gradient and earth rotation-induced Coriolis forces. The flow intensification was the reason why a large number of larvae drifted to the MAB in that year. This result suggests that in addition to larval vertical migration behaviors in the OML, the GB/GSC and MAB connectivity also depends on the intensity and duration of northeasterly winds during the fall spawning season.

It should be pointed out that scallop spawning over GB/GSC varies interannually. This variability has not been taken into account in this study. We have not considered any size-dependency of spawning either (Davies et al., 2014). No experiments were done for the case of spawning in the MAB, as it is unlikely that the larvae could be transported northward to SNE, against the prevailing southward along-shelf flow. Recent observations revealed persistent warming in the region. NECOFS shows that warming has produced a positive anomaly of water transport over the SNE shelf since 2011. An enhanced northward flow in autumn could advect larvae in the MAB to the upstream SNE region. It is worth examining these questions in the future using the 39-year hourly hind-cast NECOFS product, which can provide insights into the biophysical processes attributing to the mixing and exchanges of larvae between the GB and MAB scallop populations in the SNE region.

We did not consider the spring spawn in our experiments. The spawning time of sea scallops varies latitudinally across its range, extending from the Strait of Belle Isle, Newfoundland, to Cape Hatteras, North Carolina (Posgay, 1957; Barber and Blake, 2006; Stokesbury and Bethoney, 2020). Annual autumn spawning is typical in Newfoundland (MacDonald and Thompson, 1986), whereas semi-annual spawning is characteristic of the MAB (DuPaul et al., 1989). On GB, the autumn spawn is dominant, while spring spawning varies in magnitude and temporally (Chute et al., 2012; Hennen and Hart, 2012; Davis et al., 2014; Thompson et al., 2014; Davis et al., 2015). Depending on mortality estimates, spring-spawning contributes minimally up to about one-third of the annual total larval settlement (Davis et al., 2014). For example, Chute et al. (2012) examined 14 scallops with stable isotopes,

13 of which were fall spawned, including 6 from GB and Nantucket Shoals. The one that was spring spawned was likely spawned in the MAB. The spawning cycle, fertilization success, larval survival, and dispersion are all influenced heavily by the environment. As oceanographic conditions change on GB, spring-spawning may become increasingly important as it is in the MAB. It could also affect the larval connectivity between the GB/GSC and the MAB like that detected by Davies et al. (2014).

Our studies considered various larval swimming behaviors, which require additional field confirmation. Recently, Norton et al. (2020) examined the impact of ocean conditions on the recruitment of Dungeness crab (*Metacarcinus magister*) in the U.S. Pacific Northwest. Their studies examined six swimming behaviors. Considering these behaviors in a generalized linear model (GLM) with superior fits to the observations, they found that the ensemble solution with various swimming behaviors in the larval IBM model could improve predicting larval crab dispersion. This ensemble approach could be adopted in the larval scallop simulation, especially in a condition with various unconfirmed swimming behaviors.

## 5. Conclusions

With spawning based on multiyear-averaged abundance and distribution of adult sea scallops over GB/GSC, we examined the impacts of physical processes and larval swimming behaviors within the OML on the interannual variability of the scallop larval dispersal and settlement in the GB/GSC, SNE, and MAB regions over 1978–2016. The study was conducted using the coupled Scallop-IBM and NECOFS model. The results indicate that in addition to the flow-induced advection, larval behaviors in the OML significantly affected larval dispersal and settlement by altering the flow-induced advection experienced at different depths. The thermocline-seeking, diel or semidiurnal migration behaviors of larvae in the OML increased the larval residence time in the water column over GB/GSC. These behaviors led to persistent larval aggregations in the GB/GSC and SNE regions. In addition to larval behaviors, larval transports to the MAB were also closely related to the intensity and



duration of northeasterly wind in autumn. No functional connectivity of larvae between GB/GSC and the MAB occurred in the past 39 years, except in the autumn of 2009, during which an extreme northeasterly wind prevailed. Neglecting larval behaviors in the OML can exaggerate the connectivity scale of the GB and MAB sea scallop populations. Our studies suggest this connectivity will only matter in intense wind scenarios as expected with future climate change.

SNE is the region featuring a maximum interannual variability of larval settlement. The NECOFS has captured the climate change-induced warming over the U.S. northeastern shelf. The extreme warming at the shelfbreak off GB has significantly intensified the cross-isobath gradient of water temperature and enhanced the clockwise subtidal gyre over the bank. This change tends to increase the larval retention rate over GB/GSC, suggesting higher scallop recruitment in the future.

### Declaration of Competing Interest

The authors declare that they have no known competing financial interests or personal relationships that could have appeared to influence the work reported in this paper.

### Acknowledgment

This work was supported by the NOAA RSA Program with grant

number NA17NMF-4540042 for C. Chen, L. Zhao, P. He, R. C. Beardsley, and S. Gallagher, NA19NMF450023 for C. Chen, P. He, R. C. Beardsley, and K. Stokesbury, NOAA Fishery Climate Program with grant number NA17OAR4310273 for R. Ji and C. Davis, with WHOI subcontract number A101376 for C. Chen, and L. Zhao. The NOAA-funded IOOS NERACOOS program supported the NECOFS product under subcontract numbers NA16NOS0120023, NERACOOS A007, and NERACOOS A008. W. C. Gentleman was supported by the Natural Science and Engineering Research Council of Canada with grant number RGPIN 2016-05264. The NECOFS improvement is funded by the NSF LTER Program through the WHOI subcontract number A101354. We thank the Department of Fisheries and Oceans (DFO), Canada, for providing Canadian scallop survey data. We also would like to thank Jessica Sameoto and Freya Keyser in DFO for their kindly helps in creating and delivering a well-organized Canadian dataset available to us and NOAA scientists and staff who made the NOAA dredge survey data available for this study. Dr. Brian Rothschild has given many valuable suggestions and comments on our works. His help is greatly appreciated. We also want to thank two reviewers for their constructive comments and suggestions, which helped improve the quality of this paper.

### Appendix A. A method to calculate the thickness of the ocean mixed layer

The thickness of the surface ocean mixed layer (OML) is defined as a depth above which the water density remains essentially unchanged in the vertical. In practice, it is usually determined using a threshold approach with a criterion relative to a reference value (e.g., de Boyer Montégut et al., 2004). Here we introduced a method based on the density profile.

Defining  $H$  as the bathymetric depth at a particular geographic location,  $\rho$  as the water density that varies vertically from  $z = 0$  at the surface to  $z = -H$  at the bottom and  $\rho_o$  as the surface water density, we can estimate the mixed layer depth ( $h_m$ ) by

$$h_m = H - \sqrt{2h_{diff}/\gamma} \quad (A1)$$

where  $h_{diff} = h - \rho_o H$ ;  $h = \int_{-H}^z \rho dz$ ; and  $\gamma$  is defined as the maximum increase rate of the density with depth. Once  $\gamma$  is determined from a density profile, we can precisely estimate  $h_m$ . To demonstrate how this method work, examples are given below for three idealized cases.

Case 1: A vertically well-mixed case with a density profiler shown in Fig. A1. In this case,  $\rho$  is constant throughout the water column, so that

$$\rho = \rho_o; h = \rho_o H; \text{ and } h_{diff} = 0$$

Substituting  $h$  and  $h_{diff}$  into (A.1), we have  $h_m = H$ . Note here that  $\gamma = 0$ . For a real application, one can directly assume  $h_m$  equals the local depth.

Case 2: A stratified case with a linear density profiler shown in Fig. A2. In this case,

$$\rho = \rho_o - (\rho_H - \rho_o)z/H.$$

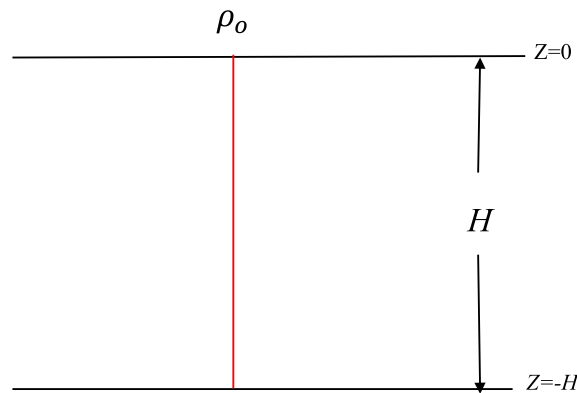


Fig. A1. Illustration of the density profile under a vertically well-mixed condition for Case 1.

Substituting it into (A.1), we have

$$h = \int_{-H}^0 [\rho_o - (\rho_H - \rho_o)z/H] dz = (\rho_H + \rho_o)z/H; h_{diff} = 0.5(\rho_H - \rho_o)H$$

Also,  $\gamma = (\rho_H - \rho_o)/H$ , so that  $h_m = H - \sqrt{2h_{diff}/\gamma} = 0$ .

Case 3: A two-layer with a density profiler shown in Fig. A3. In this case, the density profiler is given as

$$\rho = \begin{cases} \rho_o, & -h_m \leq z \leq 0 \\ \rho_o - (\rho_H - \rho_o)(z + h_m)/(H - h_m), & z \leq -h_m \end{cases}$$

and  $\gamma = (\rho_H - \rho_o)/(H - h_m)$ , then, we have

$$h = \rho_o h_m + 0.5(\rho_H + \rho_o)(H - h_m)$$

and

$$h_{diff} = h - \rho_o H = \frac{\rho_H - \rho_o}{2}(H - h_m),$$

so that

$$h_m = H - \sqrt{2h_{diff}/\gamma} = H - (H - h_m) = h_m.$$

With demonstrations from these three idealized cases, we applied this method to calculate the thickness of the OML based on the NECOFS-produced hourly density profile. The result was validated by comparing it with the simulated temperature, salinity, and density profiles at nodes of the triangular mesh. Examples are shown in Fig. A4 for selected three sites across GB. Using (A.1), we calculated  $h_m$  at these sites. They equaled 14.8, 5.0, and 9.1 m, respectively. Marking the calculated  $h_m$  using red dashed lines in the profiles, we found that they matched well with the depth of model-simulated OML.

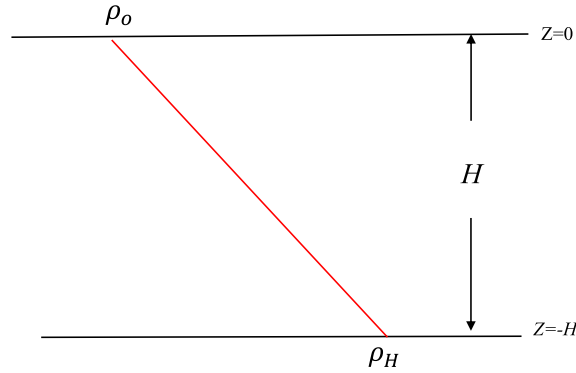


Fig. A2. Illustration of a linear density profile under a stratified condition for Case 2.

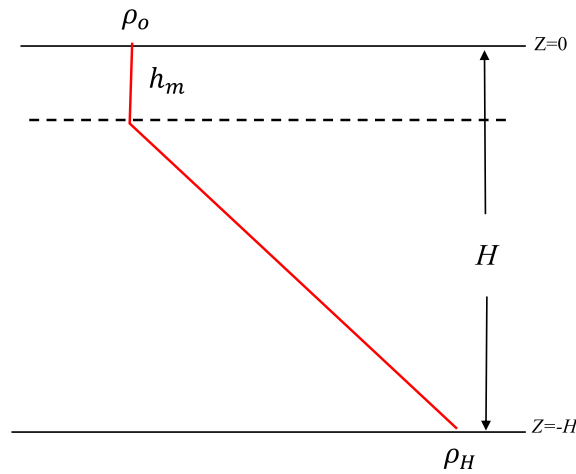
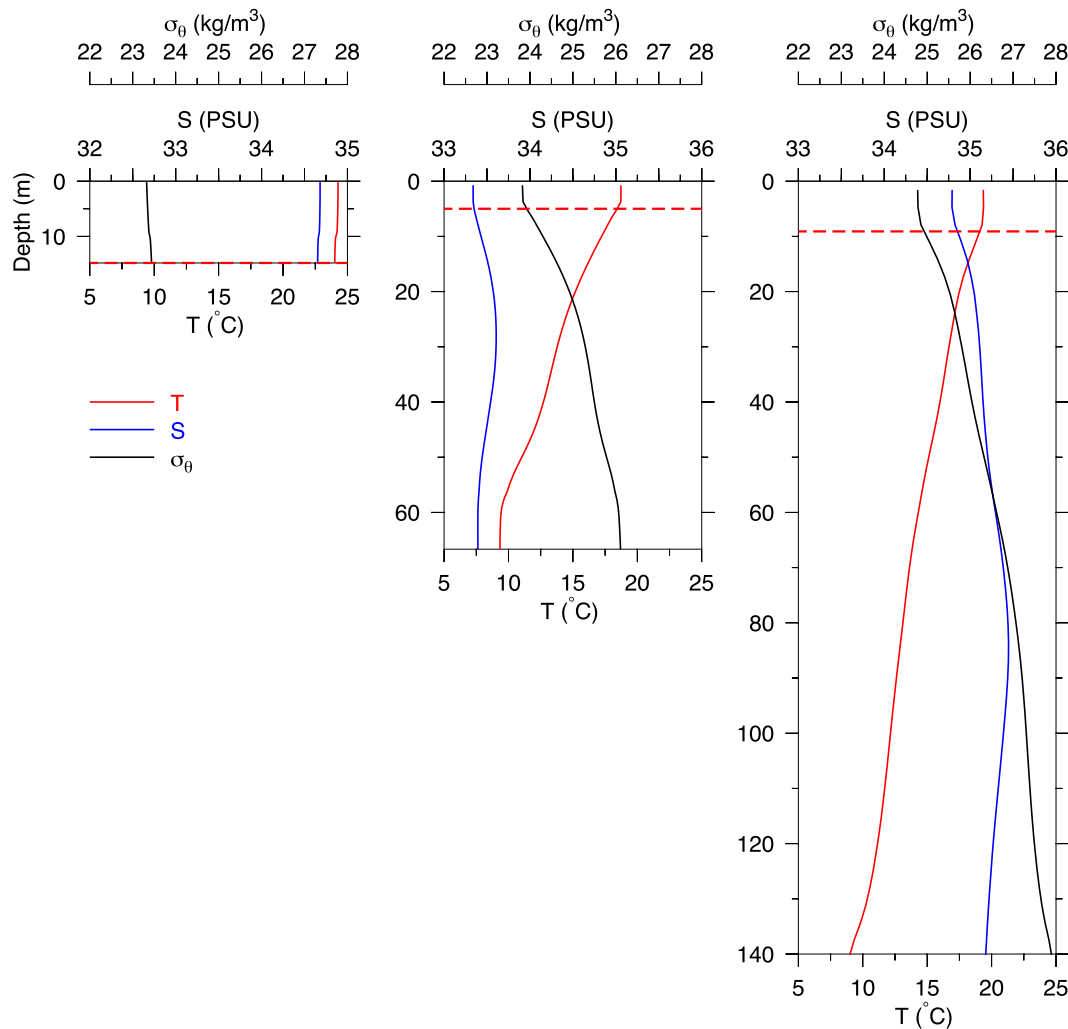


Fig. A3. Illustration of a two-layer system in which the water density is constant in the upper layer and linearly increases with depth in the lower layer for Case 3.





**Fig. A4.** Vertical profiles of sea temperature (red), salinity (blue), and density (black) at three sites across GB at 00:00 GMT, September 1, 2013. The thick dashed line represents the OML depth calculated using Eq. (A.1) in Appendix 1. (For interpretation of the references to color in this figure legend, the reader is referred to the web version of this article.)

## References

- Barber, B.J., Blake, N.J., 2006. Reproductive physiology. In: Shumway, S.E. (Ed.), *Scallops: Biology, Ecology and Aquaculture*. Elsevier, Amsterdam, pp. 377–428.
- Bartsch, J., Coombs, S.H., 2004. An individual-based model of the early life history of mackerel (*Scomber scombrus*) in the eastern North Atlantic, simulating transport, growth, and mortality. *Fish. Oceanogr.* 13, 365–379.
- Beardsley, R.C., Chen, C., Xu, Q., 2013. Coastal flooding in Scituate (MA): a FVCOM study of the Dec. 27, nor'easter. *J. Geophys. Res.-Oceans* 118. <https://doi.org/10.1002/2013JC008862>.
- Bethoney, N.D., Asci, S.C., Stokesbury, K.D.E., 2016. Implications of extremely high recruitment events into the US sea scallop fishery. *Mar. Ecol. Prog. Ser.* 547, 137–147.
- Caddy, J.F., 1975. Spatial model for an exploited shellfish population, and its application to the Georges Bank scallop fishery. *J. Fisheries Res. Board Canada* 32, 1305–1328.
- Chen, C., Liu, H., Beardsley, R.C., 2003. An unstructured, finite-volume, three-dimensional, primitive equation ocean model: application to coastal ocean and estuaries. *J. Atmos. Oceanic Technol.* 20, 159–186.
- Chen, C., Huang, H., Beardsley, R.C., Xu, Q., Limeburner, W., Cowles, G.W., Sun, Y., Qi, J., Lin, H., 2011. Tidal dynamics in the Gulf of Maine and New England Shelf: an application of FVCOM. *J. Geophys. Res.-Oceans* 116, C12010. <https://doi.org/10.1029/2011JC007054>.
- Chen, C., Gao, G., Zhang, Y., Beardsley, R.C., Lai, Z., Qi, J., Lin, H., 2016. Circulation in the Arctic Ocean: results from a high-resolution coupled ice-sea nested Global-FVCOM and Arctic-FVCOM system. *Prog. Oceanogr.* 141 (2016), 60–80. <https://doi.org/10.1016/j.pocean.2015.12.002>.
- Chen, C., Beardsley, R.C., Cowles, G., Qi, J., Lai, Z., Gao, G., Stuebe, D., Liu, H., Xu, Q., Xue, P., Ge, J., Ji, R., Hu, S., Tian, R., Huang, H., Wu, L., Lin, H., Sun, Y., Zhao, L., 2013b. An unstructured-grid, finite-volume community ocean model FVCOM user manual, 4th ed. SMASST/UMASSD Technical Report-13-0701, University of Massachusetts-Dartmouth, p. 404.
- Chen, C., Beardsley, R.C., Luettich Jr., R. A., Wang, H., Perrie, W., Xu, Q., Dohahue, A.S., Qi, J., Lin, H., Zhao, L., Kerr, P., Meng, Y., Toulany, B., 2013a. Extratropical storm inundation testbed: intermodal comparisons in Scituate, Massachusetts. *J. Geophys. Res.-Oceans* 118. <https://doi.org/10.1002/jgrc.20397>.
- Chen, C., Gao, G., Qi, J., Proshutinsky, A., Beardsley, R.C., Kowalik, Z., Lin, H., Cowles, G., 2009. A new high-resolution unstructured grid finite volume Arctic Ocean model (AO-FVCOM): an application for tidal studies. *J. Geophys. Res.-Oceans* 114, C08017. <https://doi.org/10.1029/2008JC004941>.
- Culliney, J.L., 1974. Larval development of the giant sea scallop *Placopecten magellanicus* (Gmelin). *Biol. Bull.* 147, 321–332.
- Chute, A.S., Wainwright, S.C., Hart, D.R., 2012. Timing of shell ring formation and patterns of shell growth in the sea scallop *Placopecten magellanicus* based on stable oxygen isotopes. *J. Shellfish Res.* 31 (3), 649–662.
- Cragg, S.M., 2006. Development, physiology and ecology of scallop larvae. In: Shumway, S.E., Parsons, G.J. (Eds.), *Scallops: Biology, Ecology and Aquaculture*. Elsevier, Amsterdam, pp. 45–122.
- Davis, K.T.A., Gentleman, W.C., DiBacco, C., Johnson, C.L., 2015. Fisheries closed area strengthen scallop larval settlement and connectivity among closed areas and across international open fishing grounds: a model study. *Environ. Manage.* 16. <https://doi.org/10.1007/s00267-015-0526-9>.
- Davis, K.T.A., Gentleman, W.C., Johnson, C.L., DiBacco, C., 2014. Relative contribution of bi-seasonally spawned larvae to scallop population connectivity on Georges Bank: importance of the spring spawns. *Mar. Ecol. Prog. Ser.* 10975. <https://doi.org/10.3354/meps.2004JC002378>.
- de Boyer Montégut, C., Madec, G., Fischer, A.S., Lazar, A., Iudicone, D., 2004. Mixed layer depth over the global ocean: an examination of profile data and a profile-based climatology. *J. Geophys. Res.-Oceans* 109, C12003. <https://doi.org/10.1029/2004JC002378>.
- DiBacco, C., Robert, G., Grant, J., 1995. Reproductive cycle of the sea scallop, *Placopecten magellanicus* (Gmelin, 1791), on northeast-ern Georges Bank. *J. Shellfish Res.* 14, 59–69.

- DuPaul, W., Kirkley, J., Schmitzer, A., 1989. Evidence of a semiannual reproductive cycle for the sea scallop, *Placopecten magellanicus* (Gmelin, 1791), in the mid-Atlantic region. *J. Shellfish Res.* 8, 173–178.
- Flagg, C.N., 1987. Hydrographic structure and variability. In: R.H. Backus (Ed.), *Georges Bank*, The MIT Press, pp. 108–124.
- Gallager, S.M., Mann, R., 1986. Growth and survival of larvae of *Mercenaria mercenaria* (L.) *Crassostrea virginica* (Gmelin) and *Placopecten magellanicus* relative to lipid content of eggs and broodstock conditioning. *Aquaculture* 56 (2), 105–121.
- Gallager, S.M., Mann, R., Sasaki, G.L., 1986. Lipid as an index of growth and viability in three species of bivalve larvae. *Aquaculture* 56 (2), 81–103.
- Gallager, S.M., 1988. Visual observations of particle manipulation during feeding in larvae of bivalve molluscs. *Bull. Mar. Sci.* 43 (3), 344–365.
- Gallager, S.M., 1993. Hydrodynamic disturbances produced by small zooplankton: a case study for veliger larvae of bivalve molluscs. *J. Plankton Res.* 15 (11), 1277–1296.
- Gallager, S.M., 1996. Ciliary suspension-feeding and particle selection in mollusc larvae. *J. Shellfish Res.* 15 (2), 506–510.
- Gallager, S.M., Manuel, J.L., Manning, D.A., O'Dor, R., 1996. Ontogenetic changes in the vertical distribution of scallop larvae *Placopecten magellanicus* in 9 m-deep mesocosms as a function of light, food, and temperature stratification. *Mar. Biol.* 124, 679–692.
- Gallager, S.M., 2016. Report to the Scallop PDT August 30, 2016 on scallop resource and biomass in the Closed Area II HAPC. NEFC website <http://www.nefmc.org/>.
- Gilbert, C.S., Gentleman, W.C., Johnson, C.L., DiBacco, C., Pringle, J.M., Chen, C., 2010. Modelling dispersal of sea scallop (*Placopecten magellanicus*) larvae on Georges Bank: the influence of depth-distribution, planktonic duration and spawning seasonality. *Prog. Oceanogr.* 87 (1–4), 37–48.
- Hart, D.R., 2006. Effects of sea stars and crabs on sea scallop *Placopecten magellanicus* recruitment in the Mid-Atlantic Bight (USA). *Mar. Ecol. Prog. Ser.* 306, 209–221.
- Hart, D.R., Rago, P.J., 2006. Long-term dynamics of U.S. Atlantic sea scallop *Placopecten magellanicus* populations. *N. Am. J. Fish. Manag.* 26, 490–501. <https://doi.org/10.1577/M04-116.1>.
- Hart, D.R., Chute, A.S., 2004. Essential Fish Habitat Source Document: Sea Scallop, *Placopecten magellanicus*, Life History and Habitat Characteristics, second ed. NOAA Tech. Mem. NMFS-NE-189.
- Hart, D.R., Jacobson, L.D., Tang, J., 2013. To split or not to split: assessment of Georges Bank sea scallops in the presence of marine protected areas. *Fish. Res.* 144, 74–83.
- Hart, D.R., Munroe, D.M., Caracappa, J.C., Haidvogel, D., Shank, B.V., Rudders, D.B., Klinck, J.M., Hofmann, E.E., Powell, E.N., 2020. Spillover of sea scallops from rotational closures in the Mid-Atlantic Bight (United States). *ICES J. Mar. Sci.* 77 (5), 1992–2002.
- Hennen, D.R., Hart, D.R., 2012. Shell height-to-weight relationships for Atlantic sea scallops (*Placopecten magellanicus*) in offshore U.S. waters. *J. Shellfish Res.* 31 (4), 1133–1144.
- Larsen, P.F., Lee, R.M., 1978. Observations on the abundance, distribution and growth of postlarval sea scallop, *Placopecten magellanicus*, on Georges Bank. *The Nautilus* 92, 112–116.
- Lentz, S.J., 2017. Seasonal warming of the Middle Atlantic Bight Cold Pool. *J. Geophys. Res. Oceans* 122 (2), 941–954. <https://doi.org/10.1002/2016.JC012201>.
- Lentz, S., Shearman, K., Anderson, S., Plueddemann, A., Edson, J., 2003. Evolution of stratification over the New England shelf during the Coastal Mixing and Optics study, August 1996–June 1997. *J. Geophys. Res.-Oceans* 108 (C1), 3008. <https://doi.org/10.1029/2001JC001121>.
- Li, Y., Frantoni, P.S., Chen, C., Hare, J., Sun, Y., Beardsley, R.C., Ji, R., 2015. Spatio-temporal patterns of stratification on the Northwest Atlantic shelf. *Prog. Oceanogr.* 134, 123–127.
- Li, S., Chen, C., Wu, Z., Beardsley, R.C., Li, M., 2020. Impacts of oceanic mixed layer on hurricanes: a simulation experiment with Hurricane Sandy. *e2019JC015851*. *J. Res.-Oceans* 125. <https://doi.org/10.1029/2019JC015851>.
- MacDonald, B.A., Thompson, R.J., 1986. Influence of temperature and food availability on the ecological energetics of the giant scallop *Placopecten magellanicus*. III. physiological ecology, the gametogenic cycle and scope for growth. *Mar. Biol.* 93, 37–48.
- Manuel, J.L., Gallager, S.M., Pearce, C.M., Manning, D.A., O'Dor, R.K., 1996. Veligers from different populations of sea scallop *Placopecten magellanicus* have different migration patterns. *Mar. Ecol. Prog. Ser.* 142, 147–163.
- McGarvey, R., Serchuk, F.M., McLaren, I.A., 1992. Statistics of reproduction and early life history survival of the Georges Bank sea scallop (*Placopecten magellanicus*) population. *J. Northwest Atl. Fish. Sci.* 13, 83–99.
- McGarvey, R., Serchuk, F.M., McLaren, I.A., 1993. Spatial and parent-age analysis of stock-recruitment in the Georges Bank sea scallop (*Placopecten magellanicus*) population. *Can. J. Fish. Aquat. Sci.* 50, 564–574.
- Merrill, A.R., Edwards, R.L., 1976. Observation on mollusks from a navigation buoy with special emphasis on the sea scallop *Placopecten magellanicus*. *The Nautilus* 90, 54–61.
- Mullen, D.M., Morning, J.R., 1986. Species profiles: Life histories and environmental requirements of coastal fishes and invertebrates (North Atlantic) sea scallop. *Biol. Rep. US Fish Wildlife Serv.* 1986, 21p.
- Munroe, D.M., Haidvogel, D., Caracappa, J.C., Klinck, J.M., Powell, E.N., Hofmann, E.E., Shank, B.V., Hart, D.R., 2018. Modeling larval dispersal and connectivity for Atlantic sea scallop (*Placopecten magellanicus*) in the Middle Atlantic Bight. *Fish. Res.* 208, 7–15.
- Murawski, S.A., Brown, R., Lai, H.L., Rago, P.J., Hendrickson, L., 2000. Large-scale closed areas as a fishery-management tool in temperate marine systems: The Georges Bank experience. *Bull. Mar. Sci.* 66, 775–798.
- Naidu, K.S., Robert, G., 2006. Fisheries sea scallop. *Placopecten magellanicus*. In: Shumway, S.E., Parsons, G.J. (Eds.), *Scallops: Biology, Ecology and Aquaculture*. Elsevier, Amsterdam, pp. 869–905.
- North, E.W., Schlag, Z., Hood, R.R., Li, M., Zhong, L., Goss, T., Kennedy, V.S., 2018. Vertical swimming behavior influences the dispersal of simulated oyster larvae in a coupled particle-tracking and hydrodynamic model of Chesapeake Bay. *Mar. Ecol. Prog. Ser.* 359, 99–115. <https://doi.org/10.3354/meps07317>.
- Northeast Fisheries Science Center (NFSC), 2018. 65th Northeast Regional Stock Assessment Workshop (65th SAW) Assessment Report. US Dept Commer, Northeast Fish. Sci. Cent. Ref. Doc. 18-08, 43 pp.
- Norton, E., Siedlecki, S.A., Kaplan, I.C., Hermann, A.J., Fisher, J., Morgan, C., Officer, S., Saenger, C., Alin, S.A., Newton, J., Bednarek, N., Feely, R.A., 2020. The importance of environmental exposure history in forecasting Dungeness crab megalopae, occurrence using J-SCOPE, a high-resolution model for the US Pacific Northwest. *Front. Mar. Sci.* 7, 102.
- Page, F.H., Sinclair, M., Naimie, C.E., Loder, J.W., Lozier, R.J., Berrien, P.L., Loug, R.G., 1999. Cod and haddock spawning on Georges Bank in relation to water residence times. *Fish. Oceanogr.* 8, 212–226.
- Pearce, C.M., O'Dor, R.K., Gallager, S.E., Manning, D.A., Bourget, E., 1996. Settlement of sea scallop *Placopecten magellanicus* larvae in 9 m deep mesocosms as a function of food distribution, thermoclines, depth, and substratum. *Mar. Biol.* 124 (4), 693–706.
- Pearce, C.M., Gallager, S.M., Manning, D.A., O'Dor, R.K., Bourget, E., 1998. Effect of thermoclines and turbulence on depth of larval settlement and spat recruitment of the giant scallop *Placopecten magellanicus* larvae in 9 m-deep laboratory mesocosms. *Mar. Ecol. Prog. Ser.* 165, 195–215.
- Pearce, C.M., Manuel, J.L., Gallager, S.M., Manning, D.A., O'Dor, R.K., Bourget, E., 2004. Depth and timing of settlement of veligers from different populations of giant scallop, *Placopecten magellanicus* (Gmelin), in thermally stratified mesocosms. *J. Exp. Marine Biol. Ecol.* 312, 187–214.
- Posgay, J.A., 1957. The range of the sea scallop. *The Nautilus* 71, 55–57.
- Posgay, J.A., 1976. Population assessment of the Georges Bank sea scallop stocks. *ICES Document CM 1976/K: 34*.
- Posgay, J.A., Norman, K.D., 1958. An observation on the spawning of the sea scallop, *Placopecten magellanicus* (Gmelin), on Georges Bank. *Limnol. Oceanogr.* 3, 478.
- Qi, J., Chen, C., Beardsley, R.C., Perrie, W., Cowles, G.W., Lai, Z., 2009. An unstructured-grid finite-volume surface wave model (FVCOM-SWAVE): implementation, validations and applications. *Ocean Modell.* <https://doi.org/10.1016/j.ocemod.2009.01.007>.
- Rheuban, J.E., Doney, S.C., Cooley, S.R., Hart, D.R., 2018. Projected impacts of future climate change, ocean acidification, and management on the US Atlantic sea scallop (*Placopecten magellanicus*) fishery. *PLoS ONE* 13 (9), e0203536.
- Scheffer, M., Baveco, J.M., DeAngelis, D.L., Rose, K.A., Van Nes, E.H., 1995. Super-individual a simple solution for modeling large populations on an individual basis. *Ecol. Modell.* 80, 161–170.
- Shank, B.V., Hart, D.R., Friedland, K.D., 2012. Post-settlement predation by sea stars and crabs on the sea scallop in the Mid-Atlantic Bight. *Mar. Ecol. Prog. Ser.* 468, 161–177.
- Shumway, S.E., Parsons, G.L. (Eds.), 2016. *Scallops, Biology, Ecology, Aquaculture, and Fisheries*. Elsevier, Amsterdam, Oxford and Cambridge, p. 1214.
- Silva-Serra, M.A., 1995. Early Life History Traits of *Placopecten magellanicus* (Gmelin): Behaviours, Lipid Condition and Vertical Distribution of Veligers at Micro- and Meso-scales. Ph.D. thesis. Dalhousie University, Halifax, Nova Scotia, Canada.
- Silva, M.A., O'Dor, R.K., 1988. Active depth regulation by the sea scallop larvae of *Placopecten magellanicus*? *Bullet. Can. Soc. Zool.* 19 (2), 36 (Abstract).
- Stewart, P.L., Arnold, S.H., 1994. Environmental requirements of the sea scallop (*Placopecten magellanicus*) in eastern Canada and its response to human impacts. *Can. Tech Rep. Fish. Aquat. Sci.* 2005, 1–36.
- Stokesbury, K.D.E., Harris, B.P., Marino II, M.C., Nogueira, J.I., 2004. Estimation of sea scallop abundance using a video survey in off-shore USA waters. *J. Shellfish Res.* 23, 33–44.
- Stokesbury, K.D.E., Chen, C., He, P., Zhao, L., Harris, B.P., 2015. Survey of persistent scallop aggregation and an examination of their influence on recruitment using the FVCOM oceanographic model. Final report of Sea Scallop Research under NOAA Grant Number: NA13NMF4540017.
- Stokesbury, K.D.E., O'Keefe, C.E., Harris, B.P., 2016. Fisheries Sea Scallop, *Placopecten magellanicus*. In: Shumway, S.E., Parsons, G.J. (Eds.), *Scallops: Biology, Ecology and Aquaculture*. Amsterdam: Elsevier. pp. 719–732.
- Stokesbury, K.D.E., Bethoney, N.D., 2020. How many sea scallops are there and why does it matter? *Front. Ecol. Environ.* <https://doi.org/10.1002/fee.2244>.
- Sun, Y., 2014. Long-and Short-term Oceanographic Responses to Atmospheric Forcing Over the Gulf of Maine and New England Shelf. Ph.D. Thesis. University of Massachusetts, p. 209.
- Sun, Y., Chen, C., Beardsley, R.C., Xu, Q., Qi, J., Lin, H., 2013. Impact of current-wave interaction on storm surge simulation: a case study for Hurricane Bob. *J. Geophys. Res.-Oceans* 118, 2685–2701. <https://doi.org/10.1002/jgrc.20207>.
- Sun, Y., Chen, C., Beardsley, R.C., Ullman, D., Butman, B., Lin, L., 2016. Surface circulation in Block Island Sound and adjacent coastal and shelf regions: a FVCOM-CODAR comparison. *Prog. Oceanogr.* 143 (2016), 26–45.
- Thompson, K.J., Inglis, S.D., Stokesbury, K.D.E., 2014. Identifying spawning events of the sea scallop *Placopecten magellanicus* on Georges Bank. *J. Shellfish Res.* 33 (1), 77–87.
- Tian, R.C., Chen, C., Stokesbury, K.D.E., Rothschild, B.J., Xu, Q., Hu, S., Cowles, G.W., Harris, B.P., Marino II, M.C., 2009a. Dispersal and settlement of sea scallop larvae spawned in the fishery closed areas on Georges Bank. *ICES J. Marine Sci.* 66 (10), 2155–2164. <https://doi.org/10.1093/icesjms/fsp175>.
- Tian, R.C., Chen, C., Stokesbury, K.D.E., Rothschild, B.J., Xu, Q., Cowles, G.W., Harris, B.P., Marino II, M.C., 2009b. Sensitivity analysis of sea scallop (*Placopecten magellanicus*) larvae trajectories to hydrodynamic model configuration on Georges Bank and adjacent coastal regions. *Fish. Oceanogr.* 18, 173–184.



- Tian, R.C., Chen, C., Stokesbury, K.D.E., Rothschild, B.J., Cowles, G.W., Xu, Q., Harris, B. P., Marino II, M.C., 2009c. Modeling the connectivity between sea scallop populations in the Middle Atlantic Bight and over Georges Bank. *Mar. Ecol. Prog. Ser.* 380, 147–160.
- Tremblay, M.J., 1988. A summary of the proceedings of the Halifax sea scallop workshop, August 13–14, 1987. Canadian Technical Report of Fisheries and Aquatic Sciences, No. 1605, 12 pp.
- Tremblay, M.J., Sinclair, M., 1990a. Sea scallop larvae *Placopecten magellanicus* on Georges Bank: vertical distribution in relation to water column stratification and food. *Mar. Ecol. Prog. Ser.* 61 (1–2), 1–15. <https://doi.org/10.3354/meps061001>.
- Tremblay, M.J., Sinclair, M., 1990b. Diel migration of sea scallop larvae *Placopecten magellanicus* in a shallow embayment. *Mar. Ecol. Prog. Ser.* 67, 19–25.
- Tremblay, M.J., Loder, J.W., Werner, F.E., Naimie, C.E., Page, F.H., Sinclair, M.M., 1994. Drift of sea scallop larvae *Placopecten magellanicus* on Georges Bank: a model study of the roles of mean advection, larval behavior and larval origin. *Deep-Sea Res. II* 41, 7–49.
- Van Sebille, E., Van Leeuwen, P.J., Biastoch, A., Barron, C.N., Ruijter, D., 2009. Lagrangian validation of numerical drifter trajectories using drifting buoys: application to the Agulhas system. *Ocean Model.* 29, 269–276.
- Werner, F.E., Page, F.H., Lynch, D.R., Loder, J.W., et al., 1993. Influence of mean 3-D advection and simple behavior on the distribution of cod and haddock early life stages on Georges Bank. *Fish. Oceanogr.* 2, 43–64.
- Woods, J., 2005. The Lagrangian ensemble metamodel for simulating plankton systems. *Prog. Oceanogr.* 67, 84–159.
- Zhang, Y., Chen, C., Beardsley, R.C., Gao, G., Lai, Z., Curry, B., Lee, C.M., Lin, H., Qi, J., Xu, Q., 2016a. Studies of the Canadian Arctic Archipelago water transport and its relationship to basin-local forcings: results from AO-FVCOM. *J. Geophys. Res.-Oceans* 121. <https://doi.org/10.1002/2016JC011634>, 121.
- Zhang, Y., Chen, C., Beardsley, R.C., Gao, G., Qi, J., Lin, H., 2016b. Seasonal and interannual variability of the Arctic sea ice: a comparison between AO-FVCOM and observations. *J. Geophys. Res.-Oceans* 121. <https://doi.org/10.1002/2016JC011841>.